pH Dependence of the Reduction of Dioxygen to Water by Cytochrome *c* Oxidase. 2. Branched Electron Transfer Pathways Linked by Proton Transfer†

Istvan Szundi, Ned Van Eps, and Ólöf Einarsdóttir*

Department of Chemistry and Biochemistry, University of California, Santa Cruz, California 95064

Received July 19, 2002; Revised Manuscript Received January 9, 2003

ABSTRACT: Recent time-resolved optical absorption studies in our laboratory have indicated that the putative peroxy intermediate formed during the reduction of dioxygen to water by cytochrome oxidase (**P_R**) is a pH-dependent mixture of compound **A**, **P**, and **F** [Van Eps, N., et al. (2003) *Biochemistry 42*, 5065−5073]. This conclusion is based on a kinetic analysis of flow-flash time-resolved data using a unidirectional sequential scheme with five apparent lifetimes. To account for this observation, we propose a more complex kinetic model that consists of branched pathways, one branch producing the 607 nm **P** form and the other the 580 nm **F** form. The two pathways are interconnected, and the rate of exchange between the two is pH-dependent. The kinetic analysis and testing of the new model involves a novel algebraic approach which transforms the intermediates of the complex branched scheme into intermediates comparable to those derived on the basis of a sequential model. The branched model reproduces the experimental data very well and is consistent with a variety of experimental observations. The two branches may arise from two structurally different CO or O_2 conformers or protein conformers, which could lead to different accessibilities of proton donors to the binuclear center.

The reaction kinetics of the fully reduced cytochrome oxidase with dioxygen have previously been modeled assuming a unidirectional sequential mechanism, where compound **A**[1] is converted to a putative peroxy intermediate, **P_R**. This is followed by the formation of a ferryl (**F**) and ultimately the ferric hydroxide (for reviews, see refs *1* and *2*). The reaction sequence has primarily been based on transient absorption changes detected at selected wavelengths (*3*−*6*), while time-resolved resonance Raman studies have provided structural information regarding some of the intermediates (*7*−*10*). Although single-wavelength measurements provide rather accurate apparent rates, their spectral information is limited and not optimally suited for identifying intermediate forms.

Our laboratory has focused on time-resolved optical measurements of cytochrome oxidase reaction dynamics using a multichannel diode array (*11*−*15*). This mode of detection allows the collection of spectra over a large spectral range on time scales from nanoseconds to milliseconds, thus providing both spectral and kinetic resolution. Recent multichannel flow-flash experiments in our laboratory have indicated that the putative **P_R** intermediate generated during the reaction of the fully reduced enzyme with dioxygen is not equivalent to the analogous intermediate, **P_M**, in the mixed-valence reaction or the 607 nm bench-made **P** forms (*16*).

In the preceding paper (*17*), we used a conventional unidirectional sequential mechanism [**R*** (**1**) → **R** (**2**) → **A** (**3**) → **P_R** (**4**) → **F** (**5**) → **O** (**6**)] to extract the spectra of the intermediates from the flow-flash data on the reduced enzyme. The model was tested by comparing the intermediate spectra extracted from the experimental data to the known spectral shapes of the proposed intermediates. Our results indicated that the spectrum of intermediate **4**, the putative **P_R**, was best modeled using a pH-dependent mixture of three spectra, that of compound **A** and the bench-made spectra of **P** and **F** (*17*). At low pH (6.2), intermediate **4** was modeled primarily with the spectra of **A** and **F**, with only a minor contribution (∼5%) from **P**, while at higher pH (8.5), the contribution of **P** was significantly larger (∼40%). Simultaneous formation of **P** and **F** has been observed upon addition of H_2O_2 to the oxidized enzyme, with the ratio of the two forms being dependent on both the pH and the concentration of H_2O_2 (*18*−*24*).

† This work was supported by National Institutes of Health Grant GM 53788.

* To whom correspondence should be addressed. E-mail: olof@chemistry.ucsc.edu. Phone: (831) 459-3155. Fax: (831) 459-2935.

[1] Abbreviations: Cu_A, binuclear mixed-valence copper A center; Cu_B, copper B; Fe_a, low-spin heme *a*; Fe_{a3}, heme a_3; **R***, initial Cu_B^+−CO-bound intermediate, generated following photolysis of CO from the fully reduced cytochrome *c* oxidase; **R**, fully reduced cytochrome oxidase; compound **A** (**A**), ferrous−dioxygen complex of heme a_3; **A_M**, compound **A** of the mixed-valence enzyme; **A_R**, compound **A** of the fully reduced enzyme; **P**, "peroxy" form of the enzyme in which heme a_3 has an absorption maximum at ∼607 nm when referenced against its oxidized state; **P_{CO/O_2}**, **P** generated by exposing the oxidized enzyme to a mixture of CO and O_2; **P_H**, **P** generated upon addition of H_2O_2 to the oxidized enzyme at alkaline pH; **P_M**, "peroxy" intermediate formed at the binuclear center during the reaction of the mixed-valence enzyme with dioxygen; **P_R**, putative "peroxy" intermediate formed at the binuclear center during the reaction of the fully reduced enzyme with dioxygen; **F**, ferryl form of the enzyme in which heme a_3 has an absorption maximum at ∼580 nm when referenced against its oxidized state; **F_I**, **F** in which heme *a* is oxidized and Cu_A is reduced; **F_{II}**, **F** in which heme *a* is reduced and Cu_A is oxidized; **O**, oxidized enzyme; SVD, singular value decomposition; b-spectrum, spectral changes associated with a respective first-order process; **b_{exp}** spectra, experimental b-spectra; **b_b** spectra, b-spectra associated with the branched model; **$b_{b,r}$** spectra, reduced set of b-spectra associated with the branched scheme; **Int_s**, intermediate spectra extracted on the basis of a sequential unidirectional scheme; **$Int_{b,r}$**, reduced set of intermediate spectra based on the branched scheme.

10.1021/bi020483e CCC: $25.00
Published on Web 04/08/2003

The observation that the spectrum of the putative $\mathbf{P_R}$ state can be modeled by a mixture of three spectra raises doubts about the validity of the conventional unidirectional sequential mechanism. The sequential model has been used because it is the simplest kinetic scheme that provides a straightforward mathematical solution to the kinetics and it allows calculation of intermediate spectra without assumptions. More complex kinetic schemes, including branched and parallel schemes, are mathematically underdetermined and require, in addition to the information provided by the global exponential fitting, certain assumptions for the spectra of the intermediates to be obtained. The analysis of such complex schemes, which are often degenerate, is a nontrivial kinetic problem that has not been addressed before.

In this paper, we have analyzed the reaction of fully reduced cytochrome oxidase with dioxygen using a kinetic model that consists of branched pathways. One branch produces the 607 nm **P** form and the other the 580 nm **F** form. The two branches are interconnected, and the rate of exchange between the two is pH-dependent. The testing of the branched scheme and connecting it to the traditional sequential scheme involve a novel mathematical approach based on linear algebra, which is reported here for the first time.

MATERIALS AND METHODS

The time-resolved optical absorption data on the reaction of the fully reduced enzyme with dioxygen at different pHs were described in the preceding paper (*17*). The data were analyzed using singular value decomposition (SVD) and global exponential fitting, which provided the apparent lifetimes and associated spectral changes (b-spectra) (*11*, *25*−*28*). The apparent rates were assigned to the microscopic rates of a unidirectional sequential model without back reactions, and the kinetic matrix of this linear scheme was constructed (*27*). The intermediate spectra based on this sequential model were calculated from the b-spectra and the eigenvector matrix of the kinetic matrix (*28*).

Kinetic Modeling. The details of the kinetic modeling associated with the branched pathway scheme represent an entirely new conceptual and computational approach which will be described in detail in the Results. Briefly, to test the model, a kinetic matrix of the branched pathway reaction scheme was constructed from the presumed microscopic rates, and its eigenvalues and eigenvectors were calculated. The b-spectra associated with the branched scheme were calculated from the model spectra of the presumed intermediates using the eigenvectors of the kinetic matrix of the branched scheme. The model spectra were linear combinations of the ground state spectra of the oxidized, reduced, mixed-valence CO, and fully reduced CO-bound enzyme, the oxidized spectrum of Cu_A from *Thermus thermophilus* (*29*), and the spectra of the **P** and **F** forms (*20*). The model spectra of **R*** and compound **A** were extracted from the experimental data because these could not be made on the bench. The eigenvalues and b-spectra associated with the branched scheme were compared with the experimental apparent rates and the experimental b-spectra, respectively. Degenerate and quasi-degenerate transitions of the branched reaction scheme were identified and combined into single transitions. The microscopic rates in the branched scheme were adjusted to reach satisfactory agreement between the sequential intermediate spectra and equivalent spectra generated on the basis of the branched model.

RESULTS

A Branched versus a Sequential Mechanism. When the flow-flash time-resolved data on the reaction of fully reduced cytochrome oxidase with dioxygen are analyzed, five apparent lifetimes are observed, implying at least six intermediates (*14*, *17*). The conventional reaction sequence based on a unidirectional sequential mechanism is $\mathbf{R^* \rightarrow R \rightarrow A \rightarrow P_R \rightarrow F \rightarrow O}$ (see refs *1* and *2* for reviews). However, recent kinetic analysis in our laboratory has shown that intermediate **4** (the putative $\mathbf{P_R}$) of the unidirectional sequential scheme is best modeled by a pH-dependent mixture of the dioxygen-bound intermediate (compound **A**) and the bench-made **P** and **F** forms, with only 5% of **P** present at low pH (*17*). The low-spin heme *a* is reduced in **A**, but oxidized in both **P** and **F**. The bench-made **P** form is identical to $\mathbf{P_M}$ generated upon photolysis of the mixed-valence CO-bound enzyme in the presence of dioxygen (*16*). The presence of three forms in intermediate **4** requires a mechanism more complex than a simple unidirectional sequential scheme. Schemes involving a reversible reaction between **A** and **P** were rejected (*17*) on the basis of the results of recent resonance Raman experiments which have shown that the O−O bond is already broken in **P** (*30*−*34*), making the back reaction from **P** to **A** highly unlikely.

An alternative way of producing the three components in intermediate **4** involves replacing the sequential mechanism with a scheme of two parallel pathways overlapping in time. To illustrate this, we have constructed a simple two-pathway scheme (Figure 1, middle), presumed to represent the true scheme for a hypothetical reaction. Figure 1 (top) shows the corresponding steps in a sequential scheme used to approximate the two-pathway reaction. The elements of the simple two-pathway scheme will be incorporated later into a more comprehensive branched scheme. In the two-pathway model, the amount of **A** is split into two isospectral forms [$\mathbf{A_P} = f\mathbf{A}$ and $\mathbf{A_F} = (1 - f) \times \mathbf{A}$], which have different kinetic properties. $\mathbf{A_P}$ decays into **P** in one branch, and $\mathbf{A_F}$ decays into **F** in the other branch. *f* represents the fraction of **A** going through the **P** branch. If the decay rates of $\mathbf{A_P}$ and $\mathbf{A_F}$ in the two branches were different, $\mathbf{Int_s4}$ in the sequential scheme would appear as a mixture of the **A**, **P**, and **F** forms. For example, if $\mathbf{A_P}$ decayed slower than $\mathbf{A_F}$ in the other branch, the spectral change associated with the slower decay would become "fragmented" in the exponential fit. The first fragment of the $\mathbf{A_P}$ decay would appear together with the fast $\mathbf{A_F}$ decay in a single exponential, while the remainder of the $\mathbf{A_P}$ spectral change would become part of subsequent decay processes. This concept is demonstrated quantitatively in Figure 1 (bottom), which depicts the time-dependent concentrations of the intermediates in the two individual branches (— and - - -) and the concentrations of the mixed intermediates of an equivalent sequential scheme (— — —). Seventy percent of the molecules are postulated to go through the **P** branch ($f = 0.7$) and 30% through the **F** branch.

From the time-dependent concentration profiles (Figure 1, bottom), we can make a few predictions regarding the nature of the sequential intermediates. It is clear that

Scheme 1: Branched Mechanism Used To Analyze the pH-Dependent Data[a]

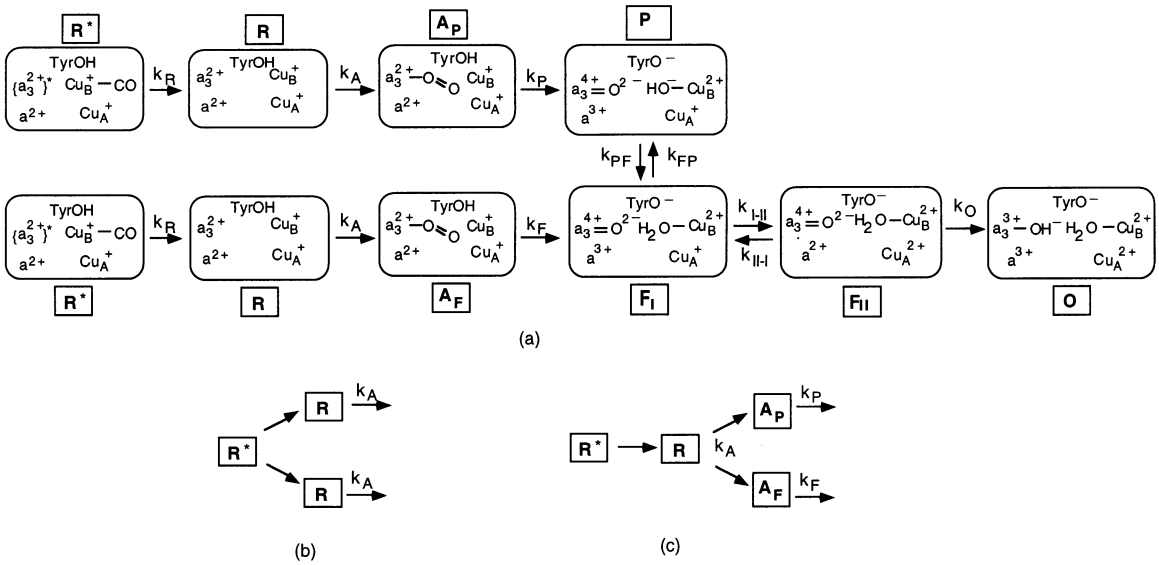

[a] All mechanisms are equivalent with the respect to the analysis and cannot be distinguished on the basis of the experimental data. (a) Branched scheme used in the analysis. (b) The same scheme as in part a except with branching occurring at **R***. (c) The same scheme as in part a except with branching occurring at **R**.

intermediate **3** (**Int$_s$3**) in the unidirectional sequential scheme (Figure 1, — — —), which is spectrally identical to **A**, does not account for the entire amount of **A**, which is the sum of the amounts of $\mathbf{A_P}$ and $\mathbf{A_F}$ (—). It is also clear that **Int$_s$4** is a composite intermediate consisting of three forms. In the time window of **Int$_s$4** of the unidirectional sequential scheme, both the **P** and **F** forms of the two-pathway scheme reach their maximum concentrations, as does the amount of the **A** form unaccounted for in **Int$_s$3**, $(\mathbf{A_P} + \mathbf{A_F}) - \mathbf{Int_s3}$. Although the data set produced by the more complex two-pathway scheme can be described mathematically by the unidirectional sequential scheme, its intermediates will appear as mixtures of the individual spectral forms of the true branched scheme. The details of how to convert a branched scheme into a unidirectional sequential one will be discussed below.

Designing the Branched Scheme. The branched mechanism used to analyze our time-resolved pH-dependent data is shown in Scheme 1. For simplicity and the convenience of the analysis, the two pathways are depicted to be independent from each other from the start (Scheme 1a). Equivalent schemes would start with a single **R*** and branch into two pathways at either **R*** (Scheme 1b) or **R** (Scheme 1c). In Scheme 1a, the **R*** and **R** intermediates are split into two isospectral and kinetically equivalent fractions, which are followed by $\mathbf{A_P}$ and **P** in the **P** branch and by $\mathbf{A_F}$ and **F** in the **F** branch. The $\mathbf{A_P}$ and $\mathbf{A_F}$ intermediates are isospectral, but kinetically not equivalent. The two branches merge at the **F** state. The conversion of **P** to **F** is reversible, although significantly forward shifted, to account for the small fraction of **P** present in intermediate **5** of the sequential scheme, **Int$_s$5**, at pH 8.5 (*17*). Note that heme *a* is oxidized and Cu_A is reduced in both **P** and $\mathbf{F_I}$, consistent with their redox states in **Int$_s$4**. In $\mathbf{F_{II}}$, heme *a* is reduced and Cu_A is oxidized. In both $\mathbf{F_I}$ and $\mathbf{F_{II}}$ heme a_3 has the same ferryl structure. It is also possible that **Int$_s$4** and **Int$_s$5** have different ferryl states, which are spectrally very similar. This alternative case will be explored in the Discussion.

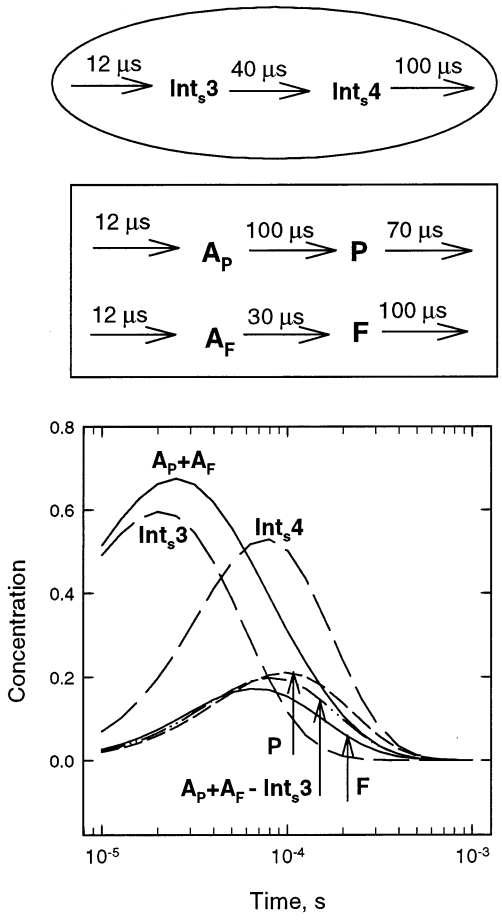

FIGURE 1: (Top) Simple unidirectional scheme showing a sequential formation of intermediate **3** (**Int$_s$3**) and intermediate **4** (**Int$_s$4**). (Middle) Simple two-branch scheme, in which compound **A** is split into two isospectral forms, $\mathbf{A_P}$ and $\mathbf{A_F}$, which decay into **P** and **F**, respectively. (Bottom) Time-dependent concentration profiles of the intermediates in the two individual branches (— and - - -) and the concentrations of the mixed intermediates of an equivalent unidirectional sequential scheme (— — —).

On the basis of the values of the experimentally observed apparent rates and the spectral composition of the intermediates extracted using the unidirectional sequential scheme (*17*), we can estimate the desired microscopic rate constants in the branched scheme. The rates will be termed either rate constants (k) or lifetimes ($\tau = 1/k$). The rates of formation of **R** (k_R) and **A** (k_A) in both branches are independent of pH and are equal to the ~1.5 and ~13 μs lifetimes, respectively, in the global exponential fit. The decay lifetimes of the two **A** intermediates are set to two different values, 30−40 and 80−100 μs, in the two branches, which match two of the experimentally observed apparent lifetimes at pH 6.2 and 7.5. Whether the **P** branch (k_P) or the **F** branch (k_F) is the slow branch cannot be determined at this point, and both alternatives are considered in our analysis. Note that the terms "slow" and "fast" refer to the rates of conversion of **A** to **P** and **A** to **F**, respectively, in the two branches and have no connection to the slow and fast forms of the oxidized enzyme. The **P**-to-**F** rate (k_{PF}) determines what fraction of **P** is observed in $\mathbf{Int_s4}$. This rate must be pH-dependent in light of the different composition of $\mathbf{Int_s4}$ observed at the different pH values and should favor the formation of **P** at high pH and **F** at low pH (*17*). The range of values for k_{PF} depends on the rate of **P** formation and also on the fraction (f) of **A** passing through the **P** branch.

The reversible step between $\mathbf{F_I}$ and $\mathbf{F_{II}}$ establishes the composition of intermediate **5**, $\mathbf{Int_s5}$, in the unidirectional sequential scheme, and the rates of the forward (k_{I-II}) and backward (k_{II-I}) steps should be adjusted to achieve the desired composition observed at the different pH values (*17*). The numerical values of these rates are difficult to predict because they are greatly affected by other rates. The rate constant of the last step (k_0), the conversion of $\mathbf{F_{II}}$ to **O**, is largely determined by the experimentally observed apparent lifetime in the millisecond range.

Data Analysis for the Branched Scheme Based on Linear Algebra. The first question that arises during the kinetic analysis concerns the number of intermediates in the scheme. Only five experimental apparent rates and six b-spectra are derived from the global exponential fit, which corresponds to six intermediates (*14*, *17*). On the other hand, the branched scheme has 10 intermediates (Scheme 1a), which reduces to eight kinetically different intermediates after the fractions of both the **R*** and **R** intermediates in the two branches are combined. Thus, the number of apparent rates of the branched scheme is initially nine and then is reduced to seven after the truly degenerate pairs of k_R and k_A are combined. It is clear that the seven apparent lifetimes and eight intermediates of the branched scheme cannot be compared directly to the five experimental apparent lifetimes and the six intermediates predicted from the global exponential fit. This obstacle can be overcome by considering the branched scheme to be quasi-degenerate or degenerate in practice. This means that the closely spaced apparent rates and the corresponding b-spectra of the branched scheme should be combined before comparing them to the corresponding experimental parameters. Note that it is a unique property of the algebraic approach that allows different schemes to be compared and the degeneracy to be treated in a quantitative way.

The second question concerns the number of microscopic rates in the branched scheme. Because of the reversible steps, the branched scheme has nine microscopic rates, and obviously, they cannot be obtained directly from the five experimental apparent rates. In mathematical terms, the kinetic problem is underdetermined and requires additional information for reasonable predictions about the reaction rates to be made. The model spectra of the proposed intermediates in the branched scheme represent this additional information. The model spectra of **R**, **P**, $\mathbf{F_I}$, $\mathbf{F_{II}}$, and **O** are the recorded spectra of cytochrome oxidase in its various redox and ligation states or linear combinations of the recorded spectra. The model spectra of **R*** and **A** are taken from the experiment because these cannot be made on the bench. The model visible spectra of the intermediates in the branched scheme, referenced against the oxidized enzyme, are shown in Figure 2.

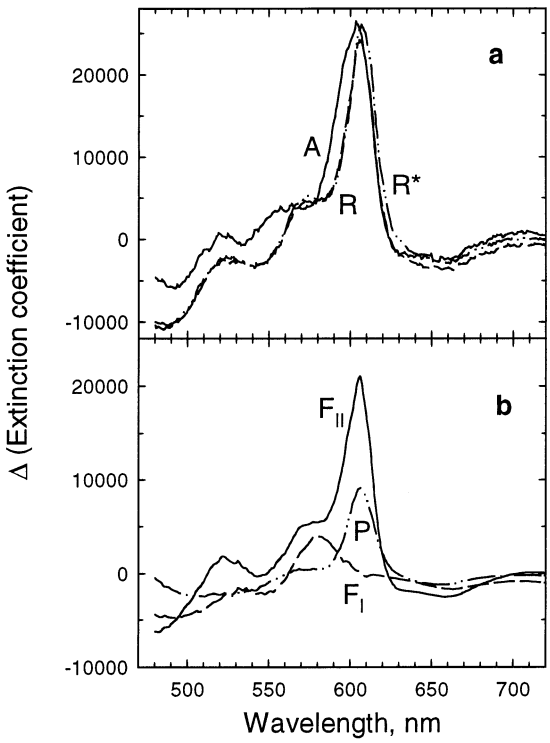

FIGURE 2: Model spectra of intermediates in the branched scheme. The spectra are referenced against the oxidized enzyme. The model spectra of **R**, **P**, $\mathbf{F_I}$, $\mathbf{F_{II}}$, and **O** are made up of linear combinations of the ground state spectra of cytochrome oxidase in its various redox and ligation states. The model spectra of **R*** and **A** are taken from the experiment because these cannot be made on the bench.

The strategy we follow in the kinetic analysis is to start from the known spectra of the intermediates in the branched scheme and find the microscopic rate constants that reproduce the experimental observations. The novel analysis method involves testing the branched scheme at the level of the b-spectra, intermediate spectra, and the experimental data set as described below.

The first step in this process involves setting up the model spectra of the intermediates in the branched scheme. Next we construct the kinetic matrix of the branched scheme ($\mathbf{K_b}$) that contains our initial predictions of the microscopic rates (k_b). Then we compute the eigenvalues (λ_b) and the scaled eigenvectors ($\mathbf{V_b}$) of the kinetic matrix. The b-spectra associated with the branched model are calculated from the model spectra of the presumed intermediates (**E**) using the eigenvectors of the kinetic matrix:

$$\mathbf{b_b} = \mathbf{E} \times \mathbf{V_b} \quad (1)$$

The λ_b and $\mathbf{b_b}$ spectra are then compared with the experimental apparent lifetimes and b-spectra, respectively, and the degenerate or quasi-degenerate $\mathbf{b_b}$ spectra are combined. This reduces the number of $\mathbf{b_b}$ spectra to the number of experimental ones:

$$\mathbf{b_{b,r}}(j) = \sum_i a_i \times \mathbf{b_b}(i) \quad (2)$$

where a_i represents the fraction of the quasi-degenerate $\mathbf{b_b}$ spectrum included in the new $\mathbf{b_{b,r}}$ spectrum. Note that a quasi-degenerate $\mathbf{b_b}$ spectrum can be split between two b-spectra of the reduced set. The reduced set of the branched scheme b-spectra ($\mathbf{b_{b,r}}$) can now be compared directly to the experimental b-spectra ($\mathbf{b_{exp}}$).

Although b-spectra are excellent tools for deriving and testing schemes, they are not always convenient for visualizing and interpreting the results. In particular, when the apparent rates are not separated sufficiently, the b-spectra are combinations of many intermediates and their amplitudes become large. Thus, the intermediate spectra produced by the mechanistic scheme are frequently easier to interpret and compare with the experimental spectral shapes of the presumed intermediates.

Normally, the intermediate spectra of a sequential unidirectional scheme, $\mathbf{Int_s}$, are calculated from the experimental b-spectra ($\mathbf{b_{exp}}$) using the eigenvector matrix ($\mathbf{V_s}$) of the kinetic matrix of the sequential scheme:

$$\mathbf{Int_s} = \mathbf{b_{exp}} \times \mathbf{V_s}^{-1} \quad (3)$$

The derived intermediate spectra are subsequently compared to model spectra of the proposed intermediates in the scheme.

An analogous calculation cannot be performed for the branched scheme, because the dimensions of the **V** matrix of the branched scheme ($\mathbf{V_b}$) and that of the experimental **b** matrix are different; there are six experimental b-spectra and eight kinetically different intermediates based on the branched scheme, as discussed above. To overcome this problem, we have developed a new approach for testing the validity of the branched scheme. First, we convert the eight intermediates of the branched scheme into six intermediates of an equivalent unidirectional sequential scheme. This can be done using the reduced set of b-spectra ($\mathbf{b_{b,r}}$) and the eigenvector matrix ($\mathbf{V_s}$) of the unidirectional sequential scheme:

$$\mathbf{Int_{b,r}} = \mathbf{b_{b,r}} \times \mathbf{V_s}^{-1} \quad (4)$$

The reduced set of intermediate spectra based on the branched scheme ($\mathbf{Int_{b,r}}$) and the intermediate spectra of the sequential scheme, $\mathbf{Int_s}$, obtained from $\mathbf{b_{exp}}$ can now be compared since both correspond to the same unidirectional scheme.

As a final test, we generate the entire set of reproduced data based on the branched scheme and compare it with the experimental data at each time delay. Note that in a traditional scheme fitting analysis method, only this last step is performed and the reasons behind poor fits remain obscure. First, we calculate the time-dependent concentrations of the intermediates in the form of a concentration matrix, **C**:

$$\mathbf{C} = \mathbf{V_b} \times \exp(\lambda_b \times \mathbf{t}) \quad (5)$$

where $\mathbf{V_b}$ and λ_b are the eigenvector matrix and the column vector of the eigenvalues of the kinetic matrix for the branched scheme, respectively, and **t** represents the row vector of the time delays. The concentration matrix is then multiplied by the matrix of the model intermediate spectra, **E**, to yield the reproduced data, $\mathbf{D_{rep}}$:

$$\mathbf{D_{rep}} = \mathbf{E} \times \mathbf{C} \quad (6)$$

which can be compared to the experimental data. After the sequence of calculations and tests is completed, the microscopic rates in the kinetic matrix of the branched scheme are adjusted until a reasonable agreement is reached between the corresponding experimental and branched model parameters and spectra. In view of the novelty and rather complex nature of the approach, the testing of the branched mechanism outlined above will be shown in detail for the pH 7.5 data. A summary of the analysis will be provided for the pH 6.2 and 8.5 data.

(I) Analysis of the pH 7.5 Data. At pH 7.5, the sequential intermediate **4**, $\mathbf{Int_s4}$, contains almost equal amounts of **A** and **F**, and slightly less **P** (*17*). We have to choose the value of k_{PF} in the branched mechanism (Scheme 1) so that the appropriate amount of **P** is observed in $\mathbf{Int_s4}$. We also must keep a fixed ratio of the k_{I-II} and k_{II-I} microscopic rates to reproduce the composition of $\mathbf{Int_s5}$.

*(A) Slow-**P**/Fast-**F** Branched Scheme.* When the **P** branch is slower than the **F** branch, the fraction of **A** in the **P** branch (*f*) must be greater than in the **F** branch for two reasons. First, a certain amount of **F** comes from the **P** branch, in addition to the fraction formed in the **F** branch, and second, the source of **A** in $\mathbf{Int_s4}$ is the slow branch of the branched scheme. Acceptable results were obtained for *f* values of 0.5−0.75, while *f* values of <0.5 did not reproduce either the apparent rates or the $\mathbf{Int_s4}$ spectrum. Table 1 shows the range of microscopic rates required to reproduce the experimental data for the slow-**P**/fast-**F** branched scheme at pH 7.5. The calculated apparent lifetimes derived from these microscopic rate constants are also listed.

The experimental apparent lifetimes at pH 7.5 are 1.5, 13, 39, and 107 μs and 1.5 ms (*17*). In our analysis using the branched model, the k_R and k_A rate constants are independent of pH and are fixed by the two fastest experimental apparent lifetimes and therefore need no further discussion. The k_F and k_P rate constants for the different values of *f* center around 2.5×10^4 and 1×10^4 s^{-1}, respectively, which correspond approximately to the experimental lifetimes of 39 and 107 μs, respectively. The **P**-to-**F** rate constant (k_{PF}) is larger than the rate of formation of **P** (k_P) and is also slightly dependent on *f*. This is because different amounts of **P** must be converted to **F** to reproduce the same composition of $\mathbf{Int_s4}$ at different *f* values. The k_P value of $2.4-2.8 \times 10^4$ s^{-1} corresponds to an apparent lifetime of slightly less than 40 μs. The back rate, k_{FP}, is set to a small value, 1×10^3 s^{-1}, and becomes important only for the pH 8.5 data. The microscopic rate constants of the reversible step between $\mathbf{F_I}$ and $\mathbf{F_{II}}$, k_{I-II} and k_{II-I}, are $1.3-1.4 \times 10^4$ and $9-10 \times 10^3$ s^{-1}, respectively. The sum of the two rate constants gives an apparent lifetime of 42−48 μs for the electron exchange

Table 1: Microscopic Rates of the Slow-**P**/Fast-**F** Branched Scheme (pH 7.5) (10^3 s^{-1})

f	k_R	k_A	k_P	k_F	k_{PF}	k_{FP}	k_{I-II}	k_{II-I}	k_O	tau (μs)
0.75	670	82	11	30	28	1	13	9	1.2	1.5, 12, 33, 33, 48, 91, 1500
0.70	670	82	9.7	30	28	1	13	9.5	1.2	1.5, 12, 33, 33, 47, 103, 1500
0.60	670	82	9.5	24	24	1	14	10	1.2	1.5, 12, 35, 42, 47, 105, 1500
0.50	670	82	9.5	20	28	1	13	9	1.3	1.5, 12, 33, 48, 50, 105, 1500

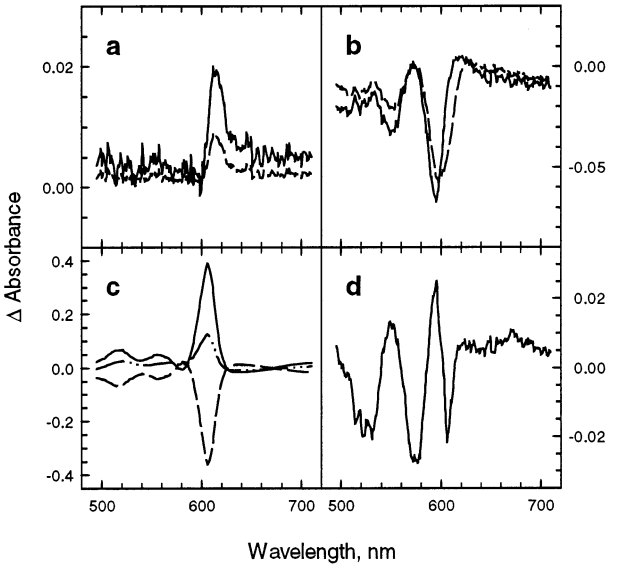

FIGURE 3: $\mathbf{b_b}$ spectra associated with the slow-**P**/fast-**F** branched scheme ($f = 0.7$) at pH 7.5. The spectra were calculated from the model spectra of the presumed intermediates (**E**) using the eigenvectors of the kinetic matrix of the branched scheme (eq 1). (a and b) $\mathbf{b_b}$ spectra associated with the 1.5 and 12 μs degenerate lifetimes, respectively. The solid lines represent the **P** branch and the dashed lines the **F** branch. (c) $\mathbf{b_b}$ spectra associated with the three quasi-degenerate lifetimes: 35 (—), 42 (− − −), and 47 μs (—••). (d) $\mathbf{b_b}$ spectrum corresponding to the 105 μs lifetime.

rate between heme *a* and Cu_A, which is in excellent agreement with the lifetime of 50 μs reported for this process upon photolysis of the two- and three-electron-reduced CO-bound enzyme (*11*, *12*, *35*−*37*). The k_O rate constant is the same, 1.2×10^3 s^{-1}, regardless of the value of *f*. It is somewhat faster than the 1.5 ms experimental apparent lifetime would predict because of the reversibility of the preceding step.

Comparing the b-spectra. Figure 3 shows the $\mathbf{b_b}$ spectra, calculated using eq 1, associated with the slow-**P**/fast-**F** branched model for an *f* of 0.7 at pH 7.5. Not shown are the $\mathbf{b_0}$ spectrum and the b-spectrum associated with the 1.5 ms lifetime, which are the same as the experimental b-spectra. Panels a and b show the $\mathbf{b_b}$ spectra associated with the degenerate 15 and 12 μs lifetimes, respectively. The different amplitudes of the two spectra in panels a and b reflect the different populations in each branch. The combination of the truly degenerate 1.5 and 12 μs lifetime pairs should correspond to their experimental counterpart (Table 1). The three lifetimes around 40 μs (Table 1) are quasi-degenerate, and the corresponding b-spectra cannot be separated in any global exponential fit. Thus, these $\mathbf{b_b}$ spectra must be combined into one before they can be compared to the experimental b-spectrum corresponding to the 39 μs lifetime. The $\mathbf{b_b}$ spectra corresponding to the 105 μs lifetime (Figure 3d) and the 1.5 ms lifetime have their experimental counterparts and can be compared directly to those spectra.

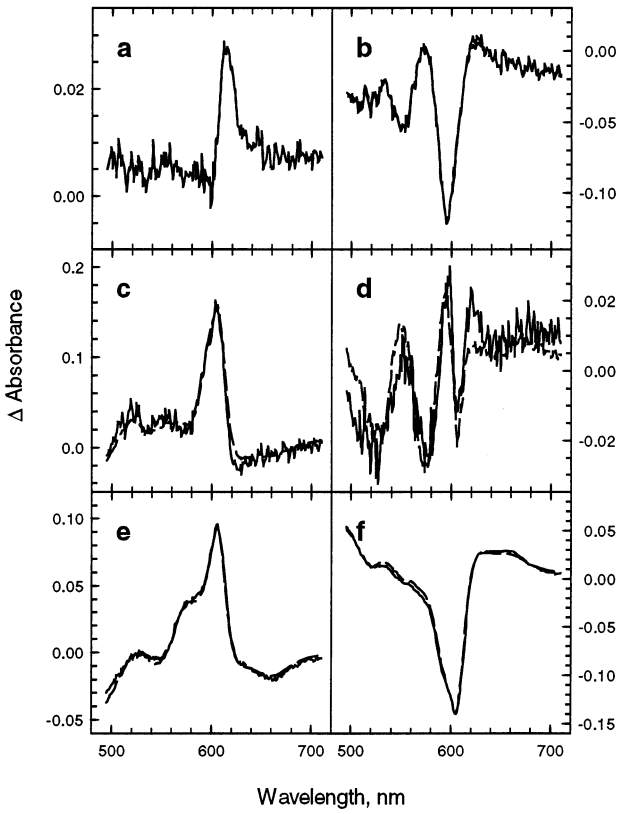

FIGURE 4: Experimental b-spectra (—) and the reduced set of b-spectra ($\mathbf{b_{b,r}}$) (− − −) reproduced by the branched slow-**P**/fast-**F** scheme at pH 7.5 ($f = 0.7$). The $\mathbf{b_{b,r}}$ spectra result from combining the degenerate or quasi-degenerate $\mathbf{b_b}$ spectra, i.e., $\mathbf{b_b}$ spectra with the same or very similar lifetimes. The apparent lifetimes associated with the experimental spectra are (a) 1.5 μs, (b) 13 μs, (c) 39 μs, (d) 107 μs, and (e) 1.5 ms. (f) Non-zero time-independent $\mathbf{b_0}$ spectrum representing the data extrapolated to infinite time.

Figure 4 shows the experimental b-spectra (—) and the reduced set of b-spectra ($\mathbf{b_{b,r}}$) (− − −) reproduced by the branched scheme. There is an excellent agreement between the $\mathbf{b_{exp}}$ and $\mathbf{b_{b,r}}$ spectra at an *f* of 0.7 and other *f* values between 0.5 and 0.75. Note that the ratio of the k_{I-II} and k_{II-I} microscopic rates in the branched scheme determines the reproduction of the 1.5 ms experimental b-spectrum, and this observation was used to fine-tune the values of these two rates. When $f < 0.5$, there were significant differences between the experimental and reproduced b-spectra.

Reproducing the Sequential Intermediate Spectra. As already discussed, the eight intermediates of the branched scheme must be converted into six intermediates of an equivalent unidirectional sequential scheme (eq 4) to test the branched model in terms of intermediate spectra. Figure 5 compares the intermediate spectra extracted from the experimental data on the basis of a unidirectional sequential scheme ($\mathbf{Int_s}$) (—) and the calculated equivalent intermediate spectra generated on the basis of the branched scheme ($\mathbf{Int_{b,r}}$) (− − −) for an *f* of 0.7. The spectra are referenced versus the oxidized enzyme. All the intermediate spectra are reproduced well for *f* values between 0.5 and 0.75, providing support for the branched model.

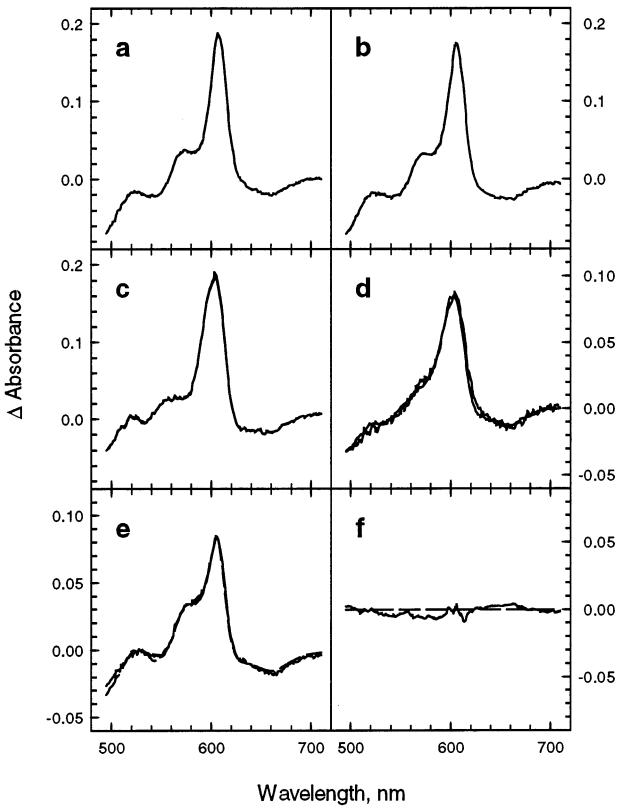

FIGURE 5: Intermediate spectra extracted from the experimental data at pH 7.5 on the basis of a unidirectional sequential scheme (**Int$_s$**) (—) and calculated equivalent intermediate spectra generated on the basis of the slow-**P**/fast-**F** branched scheme (**Int$_{b,r}$**) (– – –). **Int$_s$** spectra were derived from the experimental b-spectra using the eigenvector matrix (**V$_s$**) of the kinetic matrix of the sequential scheme (eq 3). **Int$_{b,r}$** spectra were calculated on the basis of the reduced set of b-spectra (**b$_{b,r}$**) and **V$_s$** (eq 4) for an *f* of 0.7. Spectra of intermediates **1**–**6** are shown in panels a–f, respectively. The spectra are referenced vs the oxidized enzyme.

Table 2: Microscopic Rates of the Fast-**P**/Slow-**F** Branched Scheme (pH 7.5) (10^3 s^{-1})

f	k_R	k_A	k_P	k_F	k_{PF}	k_{FP}	k_{I-II}	k_{II-I}	k_O	tau (μs)
0.25	670	82	30	10.5	10	1	11.7	8	1.2	1.5, 12, 33, 47, 95, 101, 1500
0.30	670	82	30	10	9	1	14	10	1.2	1.5, 12, 33, 39, 100, 109, 1500
0.40	670	82	33	10	7	1	14	10	1.2	1.5, 12, 30, 39, 100, 138, 1500
0.50	670	82	20	9.5	10	1	13	9	1.3	1.5, 12, 42, 50, 100, 105, 1500

*(B) Fast-**P**/Slow-**F** Branched Scheme*. In this alternative version of the branched scheme, most of **A** decays in the **F** branch, while a much smaller fraction goes through the **P** branch. Therefore, it is expected that reasonable fits will only be observed for *f* values of <0.5. Table 2 shows the range of microscopic rate constants required to reproduce the experimental data for the fast-**P**/slow-**F** branched scheme at pH 7.5. The calculated apparent lifetimes are also listed.

The first two rates, k_R and k_A, are fixed as before. When $f = 0.25-0.4$, k_P and k_F fall into narrow ranges of $3.0-3.3 \times 10^4$ and $9.5-10.5 \times 10^3$ s^{-1}, respectively, which correspond approximately to experimental lifetimes of 39 and 107 μs, respectively. The **P**-to-**F** rate constant, k_{PF} ($7-10 \times 10^3$ s^{-1}), is now smaller than the rate of formation of **P**, and is also slightly dependent on *f*. Its value corresponds to an apparent lifetime of around 100 μs, which is close to the rate of **F** formation (k_F) in the **F** branch. The back rate, k_{FP}, is set to the same small value as before (1×10^3 s^{-1}). The microscopic rate constants for the electron exchange between heme *a* and Cu_A (k_{I-II} and k_{II-I}) and for the last step (k_O) are approximately the same as for the slow-**P**/fast-**F** combination. When $f > 0.5$, the rate of formation of **P** would have to be decreased to prevent too much **P** from being produced in a short time. However, with a slower rate of formation of **P**, the 39 μs experimental apparent lifetime and the spectrum of **Int$_s$4** are no longer reproduced.

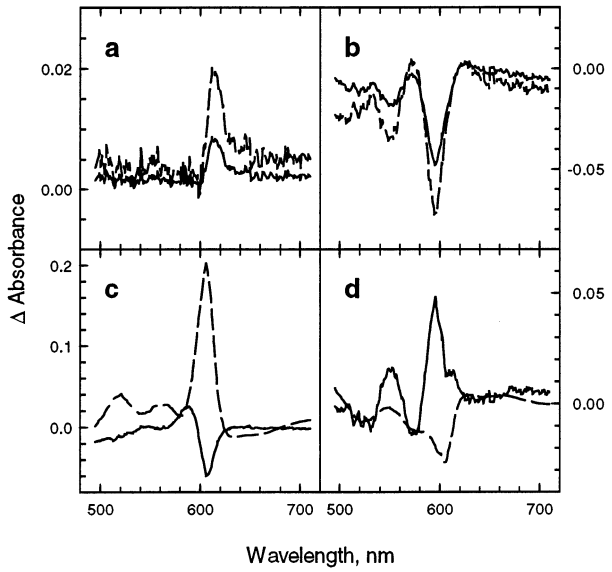

FIGURE 6: **b$_b$** spectra associated with the fast-**P**/slow-**F** branched scheme ($f = 0.3$) at pH 7.5. The spectra were calculated from the model spectra of the presumed intermediates (**E**) using the eigenvectors of the kinetic matrix of the branched scheme (eq 1). (a and b) **b$_b$** spectra associated with the 1.5 and 12 μs degenerate lifetimes, respectively. The solid lines represent the **P** branch and the dashed lines the **F** branch. (c) **b$_b$** spectra associated with two quasi-degenerate lifetimes of 33 (—) and 39 μs (– – –). (d) **b$_b$** spectra corresponding to quasi-degenerate lifetimes of 100 (—) and 109 μs (– – –).

Comparing the b-spectra. The **b$_b$** spectra corresponding to the first eight apparent lifetimes in the branched scheme (Table 2) are shown in Figure 6 for an *f* of 0.3. These include the truly degenerate pairs, 1.5 μs (panel a) and 12 μs (panel b), and the quasi-degenerate pairs, 33 and 39 μs (panel c) and 100 and 109 μs (panel d). All four pairs must be combined before they can be compared to the experimental b-spectra. The experimental b-spectra and the reduced set of b-spectra reproduced by the branched scheme (**b$_{b,r}$**) are compared in Figure 7. The 1.5 ms experimental b-spectrum is reproduced in a manner analogous to that described above because the k_{I-II} and k_{II-I} microscopic rates are very similar in the two versions of the branched scheme. The agreement between the experimental b-spectra and the **b$_{b,r}$** spectra at $f = 0.3$ is excellent, as is the case for other *f* values between 0.25 and 0.4.

Reproducing the Sequential Intermediate Spectra. The spectra of the intermediates extracted on the basis of a unidirectional sequential scheme (**Int$_s$**) and the equivalent intermediate spectra generated on the basis of the branched scheme (**Int$_{b,r}$**) are compared in Figure 8 for an *f* of 0.3. All the intermediates are reproduced well for *f* values of 0.25–0.5.

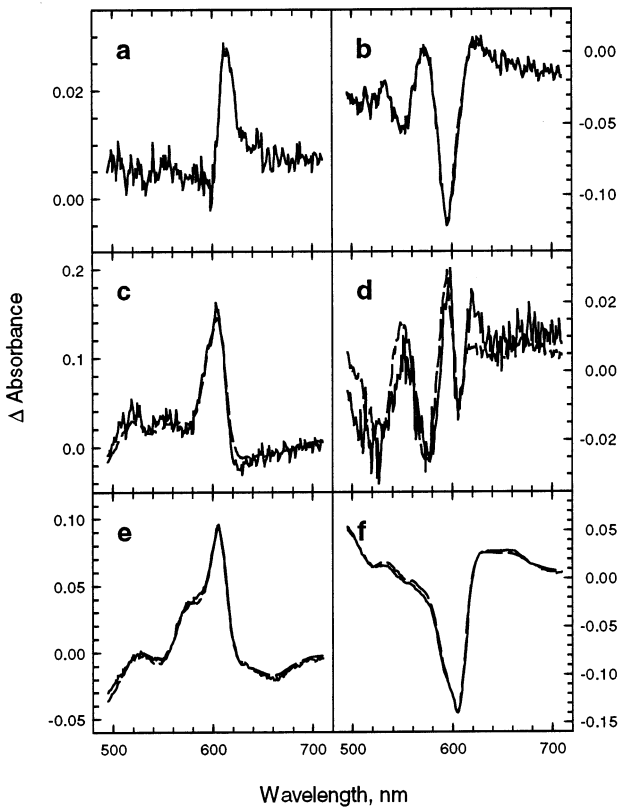

FIGURE 7: Experimental b-spectra (—) and the reduced set of b-spectra ($\mathbf{b_{b,r}}$) (— — —) reproduced by the branched fast-**P**/slow-**F** scheme at pH 7.5 ($f = 0.3$). The $\mathbf{b_{b,r}}$ spectra result from combining the degenerate or quasi-degenerate $\mathbf{b_b}$ spectra, i.e., $\mathbf{b_b}$ spectra with the same or very similar lifetimes. The apparent lifetimes associated with the experimental spectra were (a) 1.5 μs, (b) 13 μs, (c) 39 μs, (d) 107 μs, and (e) 1.5 ms. (f) Non-zero time-independent $\mathbf{b_0}$ spectrum representing the data extrapolated to infinite time.

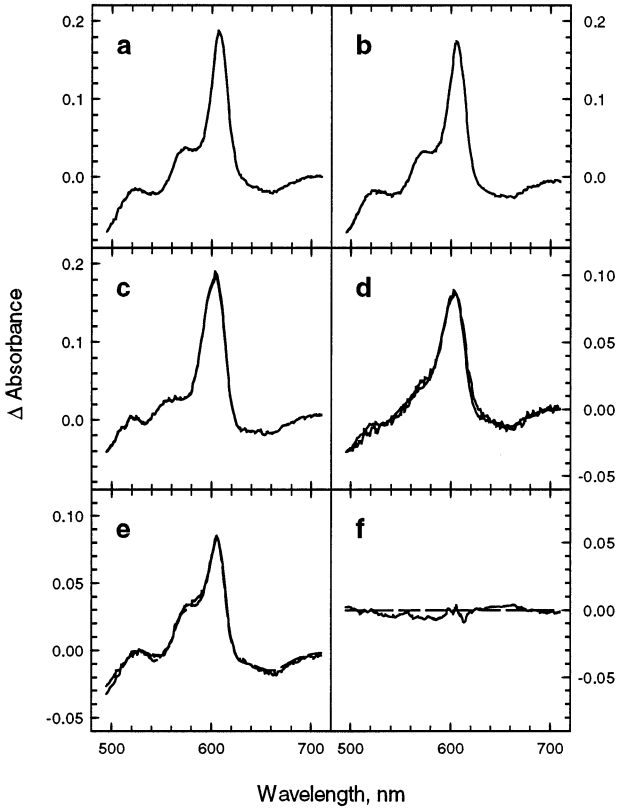

FIGURE 8: Intermediate spectra extracted from the experimental data at pH 7.5 on the basis of a unidirectional sequential scheme ($\mathbf{Int_s}$) (—) and calculated equivalent intermediate spectra generated on the basis of the fast-**P**/slow-**F** branched scheme ($\mathbf{Int_{b,r}}$) (— — —). $\mathbf{Int_s}$ spectra were derived from the experimental b-spectra using the eigenvector matrix ($\mathbf{V_s}$) of the kinetic matrix of the sequential scheme (eq 3). $\mathbf{Int_{b,r}}$ spectra were calculated on the basis of the reduced set of b-spectra ($\mathbf{b_{b,r}}$) and $\mathbf{V_s}$ (eq 4) for an f of 0.3. Spectra of intermediates **1**−**6** are shown in panels a−f, respectively. The spectra are referenced vs the oxidized enzyme.

(II) Analysis of the pH 6.2 Data. At pH 6.2, intermediate **4** of the unidirectional scheme, $\mathbf{Int_s4}$, contains almost equal amounts of **A** and **F**, with very little **P** present (*17*). This composition requires the **P**-to-**F** rate (k_{PF}) to be much faster than the rate of formation of **P**, and it is expected that this fast rate may produce an apparent lifetime approaching that of oxygen binding. The microscopic rate constants required to reproduce the data at pH 6.2 for both the slow-**P**/fast-**F** and fast-**P**/slow-**F** schemes are shown in Table 3 (top and bottom, respectively) along with the calculated apparent lifetimes. The five experimental apparent lifetimes at pH 6.2 were 1.5 μs, 13 μs, 34 μs, 80 μs, and 1.1 ms (*17*).

*Slow-**P**/Fast-**F** Branched Scheme.* The fraction of **A** in the **P** branch, f, should be substantially larger than in the **F** branch since the source of **A** in $\mathbf{Int_s4}$ is the slow branch. Practically all of the $\mathbf{A_P}$ that decays to **P** ends up in **F**; therefore, the amount of **F** formed through the fast **F** branch should be kept small. The fraction of molecules going through the **P** branch that satisfactorily reproduces the data at pH 6.2 is within a narrow range ($f = 0.7-0.85$). The k_F and k_P rates are set close to 3×10^4 and 1.2×10^4 s^{-1}, respectively, which correspond roughly to the experimental lifetimes of 34 and 80 μs, respectively. For f values of <0.7, the k_F and k_P rates become too slow and no longer match the apparent rates (Table 3, top). The same value of k_{PF} (7×10^4 s^{-1}) can be used for all the f values. The back rate, k_{FP}, is set to 1×10^3 s^{-1}, which is too small to influence the fit. The apparent lifetime produced by these two rates is 14 μs. The microscopic rates of the reversible step between $\mathbf{F_I}$ and $\mathbf{F_{II}}$ are as follows: $k_{I-II} = 1.8-2.0 \times 10^4$ s^{-1} and $k_{II-I} = 9-10 \times 10^3$ s^{-1}. The sum of the two rates gives an apparent lifetime of 33−37 μs for the electron exchange rate between heme *a* and Cu_A, which is slightly faster than that at pH 7.5. The rate of the final step is 1.4×10^3 s^{-1}, which in combination with the reversible step preceding it gives an apparent lifetime of 1.1 ms.

Table 3: Microscopic Rates of the Slow-**P**/Fast-**F** (top) or Fast-**P**/Slow-**F** (bottom) Branched Scheme (pH 6.2) (10^3 s^{-1})

f	k_R	k_A	k_P	k_F	k_{PF}	k_{FP}	k_{I-II}	k_{II-I}	k_O	tau (μs)
0.85	670	82	14	30	70	1	20	10	1.4	1.5, 12, 14, 33, 33, 71, 1100
0.80	670	82	13	30	70	1	18	9	1.4	1.5, 12, 14, 33, 37, 77, 1100
0.75	670	82	12.5	30	70	1	18	9	1.4	1.5, 12, 14, 33, 37, 80, 1100
0.70	670	82	12	30	70	1	18	9	1.4	1.5, 12, 14, 33, 37, 83, 1100
0.15	670	82	30	13	70	1	17	8	1.4	1.5, 12, 14, 33, 40, 77, 1100
0.25	670	82	30	12	70	1	17	8	1.4	1.5, 12, 14, 33, 40, 83, 1100
0.35	670	82	30	11	70	1	17	8	1.4	1.5, 12, 14, 33, 40, 91, 1100

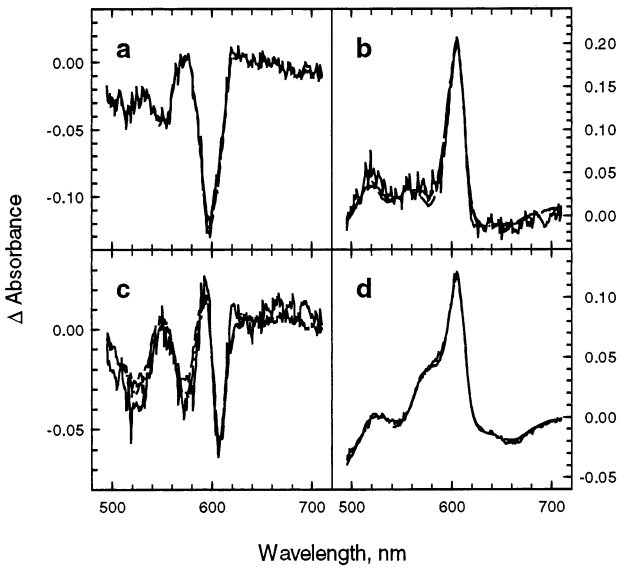

FIGURE 9: Experimental b-spectra (—) and the reduced set of b-spectra ($\mathbf{b_{b,r}}$) reproduced by the branched slow-**P**/fast-**F** scheme [$f = 0.8$ (—••)] and the fast-**P**/slow-**F** scheme [$f = 0.25$ (— — —)] at pH 6.2. The b-spectrum associated with the 1.5 μs process is omitted. The $\mathbf{b_{b,r}}$ spectra result from combining the degenerate or quasi-degenerate $\mathbf{b_b}$ spectra, i.e., $\mathbf{b_b}$ spectra with the same or very similar lifetimes. The apparent lifetimes associated with the experimental spectra were (a) 13 μs, (b) 34 μs, (c) 80 μs, and (d) 1.1 ms.

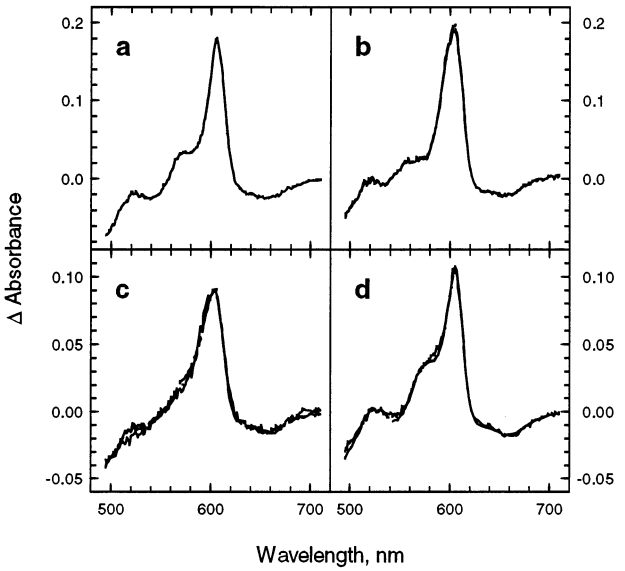

FIGURE 10: Intermediate spectra extracted from the experimental data at pH 6.2 on the basis of a unidirectional sequential scheme ($\mathbf{Int_s}$) (—) and calculated equivalent intermediate spectra ($\mathbf{Int_{b,r}}$) generated on the basis of the slow-**P**/fast-**F** branched scheme [$f = 0.8$ (—••)] and the fast-**P**/slow-**F** branched scheme [$f = 0.25$ (— — —)]. $\mathbf{Int_s}$ spectra were derived from the experimental b-spectra using the eigenvector matrix ($\mathbf{V_s}$) of the kinetic matrix of the sequential scheme (eq 3). $\mathbf{Int_{b,r}}$ spectra were calculated on the basis of the reduced set of b-spectra ($\mathbf{b_{b,r}}$) and $\mathbf{V_s}$ (eq 4). Spectra of intermediates **2**—**5** are shown in panels a—d, respectively. The spectra are referenced vs the oxidized enzyme.

*Fast-**P**/Slow-**F** Branched Scheme.* In this version of the branched scheme, most of **A** decays in the **F** branch and only a small fraction in the **P** branch. Acceptable fits are obtained only for f values of 0.15—0.35. Interestingly, the microscopic rates are almost identical to those for the slow-**P**/fast-**F** version, except the values of the k_P and k_F rate constants are interchanged (Table 3).

Comparing the b-spectra. The seven apparent lifetimes of the branched slow-**P**/fast-**F** scheme at pH 6.2 after combining the truly degenerate pairs are 1.5, 12, 14, 33, 33—37, and 71—83 μs and 1.1 ms (Table 3, top). Similar apparent lifetimes are observed for the fast-**P**/slow-**F** version (1.5, 12, 14, 33—40, and 77—91 μs and 1.1 ms) (Table 3, bottom). As shown for pH 7.5, degenerate and quasi-degenerate $\mathbf{b_b}$ spectra must be combined before a comparison with the experimental b-spectra can be made. For the slow-**P**/fast-**F** combination, most of the 14 μs $\mathbf{b_b}$ spectrum (80%) must be combined with the 12 μs degenerate pair to reproduce the 13 μs experimental b-spectrum. The remaining 20%, along with the 33 and 37 μs $\mathbf{b_b}$ spectra, reproduce the 34 μs experimental b-spectrum satisfactorily. The $\mathbf{b_b}$ spectrum associated with the 80 μs lifetime agrees with the 80 μs experimental b-spectrum. Figure 9 shows the experimental b-spectra (—) and the reduced set of b-spectra, $\mathbf{b_{b,r}}$, for the slow-**P**/fast-**F** scheme (—••) for an f of 0.8.

When the $\mathbf{b_b}$ spectra associated with the seven apparent lifetimes for the fast-**P**/slow-**F** scheme are compared for an f of 0.25, we find a number of quasi-degeneracies. Combining most of the 14 μs $\mathbf{b_b}$ spectrum (80%) with the 12 μs $\mathbf{b_b}$ spectrum reproduces the 13 μs experimental b-spectrum. The remaining 20% of the 14 μs $\mathbf{b_b}$ spectrum, almost all (90%) of the 40 μs $\mathbf{b_b}$ spectrum, and the 33 μs $\mathbf{b_b}$ spectrum are required to reproduce the 34 μs experimental b-spectrum. The remaining 10% of the 40 μs $\mathbf{b_b}$ spectrum is added to the 83 μs $\mathbf{b_b}$ spectrum to match the 80 μs experimental b-spectrum. Figure 9 (— — —) shows the reduced set of b-spectra, $\mathbf{b_{b,r}}$, for the fast-**P**/slow-**F** version. It is clear that the $\mathbf{b_{b,r}}$ spectra based on the slow-**P**/fast-**F** (—••) or fast-**P**/slow-**F** branched model (— — —) are in excellent agreement with the experimental b-spectra (—), supporting the microscopic rates in the branched model.

Reproducing the Sequential Intermediate Spectra. The reduced number of intermediate spectra ($\mathbf{Int_{b,r}}$) were calculated from the reduced set of b-spectra using the eigenvector matrix ($\mathbf{V_s}$) of the kinetic matrix of the unidirectional sequential scheme (eq 4) as discussed above for the analysis of the pH 7.5 data. Figure 10 compares the reproduced spectra of intermediates **2**—**5** of the slow-**P**/fast-**F** branched scheme (—••) and fast-**P**/slow-**F** scheme (— — —) to the intermediates derived from the experimental b-spectra based on a unidirectional sequential model, $\mathbf{Int_s}$ (—). To reproduce the spectrum of intermediate **5**, the equilibrium between $\mathbf{F_I}$ and $\mathbf{F_{II}}$ must be significantly more forward-shifted than that observed at pH 7.5. The branched scheme reproduces the experimental intermediate spectra very well at f values of 0.7—0.85 for the slow-**P**/fast-**F** version and at f values of 0.15—0.35 for the fast-**P**/slow-**F** alternative.

(III) Analysis of the pH 8.5 Data. The first three experimental apparent lifetimes at pH 8.5 are 1.5, 13, and 36 μs and do not differ significantly from the ones observed at lower pH values (*14*, *17*). However, the last two processes, 240 μs and 2.4 ms, are twice as slow as the corresponding processes at pH 7.5, in agreement with previous studies (*4*, *38*, *39*). Intermediate **4**, extracted on the basis of the unidirectional sequential scheme ($\mathbf{Int_s4}$), contains nearly equal amounts of the **A**, **P**, and **F** forms at pH 8.5, similar to that observed at pH 7.5 (*17*). This implies that the fraction

Table 4: Microscopic Rates of the Slow-**P**/Fast-**F** (top) and Fast-**P**/Slow-**F** (bottom) Branched Scheme (pH 8.5) (10^3 s^{-1})

f	k_R	k_A	k_P	k_F	k_{PF}	k_{FP}	k_{I-II}	k_{II-I}	k_O	tau (μs)
0.70	670	82	14	33	5	1	10	11	1.1	1.5, 12, 30, 45, 71, 180, 2300
0.65	670	82	12	30	4	1	9	10	1.1	1.5, 12, 33, 52, 83, 230, 2200
0.60	670	82	10	30	4	1	8	8	1.1	1.5, 12, 33, 58, 100, 230, 2200
0.30	670	82	30	12	4	1	9	9.5	1.1	1.5, 12, 33, 51, 83, 220, 2200
0.40	670	82	30	10	4	1	9	9.5	1.1	1.5, 12, 33, 51, 100, 220, 2200

f and the k_F and k_P rates used at pH 7.5 can also be applied here. However, as expected, the values of these rate constants at pH 7.5 do not yield the 240 μs experimental apparent lifetime, but rather a shorter one around 100 μs. Note that the 240 μs apparent lifetime at pH 8.5 was observed in single-wavelength traces in the near-infrared region (835 nm), while the multiwavelength data in the visible region were somewhat more consistent with a shorter lifetime of ~100 μs (*17*). Because the latter had a much larger uncertainty, the 240 μs lifetime was designated as the fourth apparent lifetime. Moreover, the near-infrared spectral region most accurately reflects the change in the Cu_A oxidation state. The possibility of a sixth apparent lifetime was not considered at that time.

The branched scheme can account for both the 100 μs apparent lifetime observed in the visible region and the 240 μs lifetime in the near-infrared region. The 100 μs lifetime is associated with the oxidation of heme *a* and thus is the dominant lifetime in the visible region, while the 240 μs apparent lifetime is assigned to the **P**-to-**F** rate (k_{PF}), and not to the reversible step between $\mathbf{F_I}$ and $\mathbf{F_{II}}$. This may seem counterintuitive since the oxidation of Cu_A happens in the latter step. However, increasing the lifetime (reducing the rate) of the reversible $\mathbf{F_I}$-to-$\mathbf{F_{II}}$ step beyond 60 μs is inconsistent with the time course at 604 nm. The characteristic steplike shape of the 604 nm trace (*39*) can only be reproduced by a relatively fast rate of electron exchange between heme *a* and Cu_A. Because the relatively fast $\mathbf{F_I}$-to-$\mathbf{F_{II}}$ reversible process follows a slower step, the conversion of **P** to **F**, the Cu_A oxidation is observed in the near-infrared region with the rate of the slower step, hence the 240 μs lifetime. Note that the rate of the **P**-to-**F** transition also increased at pH 6.2 compared to pH 7.5.

*Slow-**P**/Fast-**F** Branched Scheme.* The microscopic rate constants for the slow-**P**/fast-**F** and fast-**P**/slow-**F** branched schemes at pH 8.5 are shown in Table 4 (top and bottom, respectively), along with the calculated apparent lifetimes. The k_F and k_P rates are set close to 3×10^4 and 1×10^4 s^{-1}, respectively, which correspond to lifetimes of 34 and 100 μs, respectively. The composition of intermediate **4** (**Int$_s$4**) requires that f be >0.5. The decay of **P** is slower than its formation, and most of $\mathbf{A_P}$ that decays to **P** stays in **P** for up to 200 μs. The fraction of molecules going through the **P** branch that satisfactorily reproduces the data at pH 8.5 for the slow-**P**/fast-**F** scheme is within a narrow range (f = 0.6−0.7). To satisfactorily model sequential intermediate **5** at pH 8.5, including the desired amount of **P**, the k_{PF} and k_{FP} rates are set to 4×10^3 and 1×10^3 s^{-1}, respectively. The microscopic rates of the reversible step between $\mathbf{F_I}$ and $\mathbf{F_{II}}$ are both $8-10 \times 10^3$ s^{-1}. The sum of the two rates gives an apparent lifetime of 45−58 μs for the electron exchange between heme *a* and Cu_A, which is somewhat slower than at lower pH. The rate of the final step is 1.1×10^3 s^{-1}, which gives an apparent lifetime of 2.2−2.4 ms depending on the rate of the reversible step preceding it.

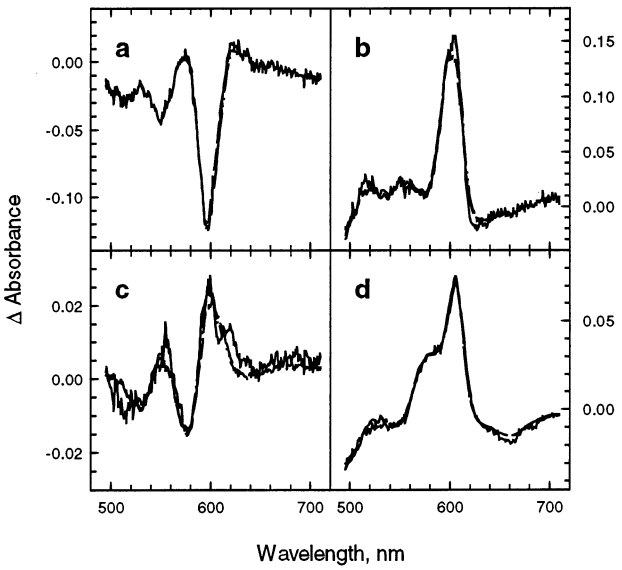

FIGURE 11: Experimental b-spectra (—) and the reduced set of b-spectra ($\mathbf{b_{b,r}}$) reproduced by the branched slow-**P**/fast-**F** scheme [f = 0.6 (—••)] and the fast-**P**/slow-**F** scheme [f = 0.4 (— — —)] at pH 8.5. The $\mathbf{b_{b,r}}$ spectra result from combining the degenerate or quasi-degenerate $\mathbf{b_b}$ spectra, i.e., $\mathbf{b_b}$ spectra with the same or very similar lifetimes. The apparent lifetimes associated with the experimental spectra were (a) 13 μs, (b) 36 μs, (c) 240 μs, and (d) 2.4 ms.

*Fast-**P**/Slow-**F** Branched Scheme.* Because of the slow rate of conversion between the **P** branch and the **F** branch at this pH, nearly acceptable fits can be obtained by merely interchanging the number of molecules going through each branch and interchanging the values of k_P and k_F found for the slow-**P**/fast-**F** scheme. The refined microscopic rates for f values of 0.3−0.4 are shown in Table 4 (bottom).

Comparing the b-spectra. The seven apparent lifetimes of the branched slow-**P**/fast-**F** scheme after combining the truly degenerate pairs are 1.5, 12, 30−33, 45−58, 71−100, and 180−230 μs and 2.2−2.3 ms (Table 4, top). The quasi-degenerate lifetimes, 30−33, 45−58, 71−100, and 180−230 μs, must be combined into two to reproduce the 36 and 240 μs experimental b-spectra. For an f of 0.6, the 33 μs $\mathbf{b_b}$ spectrum is combined with 70% of the 52 μs $\mathbf{b_b}$ spectrum and 40% of the 83 μs $\mathbf{b_b}$ spectrum to reproduce the 36 μs experimental b-spectrum. The remaining parts of the three $\mathbf{b_b}$ spectra and the 230 μs $\mathbf{b_b}$ spectrum reproduce the 240 μs experimental b-spectrum reasonably well. As demonstrated in Figure 11 for an f of 0.6, the agreement between the experimental b-spectra (—) and the reduced set, $\mathbf{b_{b,r}}$ (—••), for the slow-**P**/fast-**F** scheme is good. A similarly good fit was observed at other f values between 0.6 and 0.7.

The quasi-degeneracy of the apparent lifetimes based on the branched fast-**P**/slow-**F** model (Table 4, bottom) is very similar to the one described above for the slow-**P**/fast-**F** scheme. For f values of 0.3−0.4, the 34 μs experimental b-spectrum is reproduced by combining the 33 μs $\mathbf{b_b}$ spectrum with 80% of the 50 μs $\mathbf{b_b}$ spectrum and 50% of

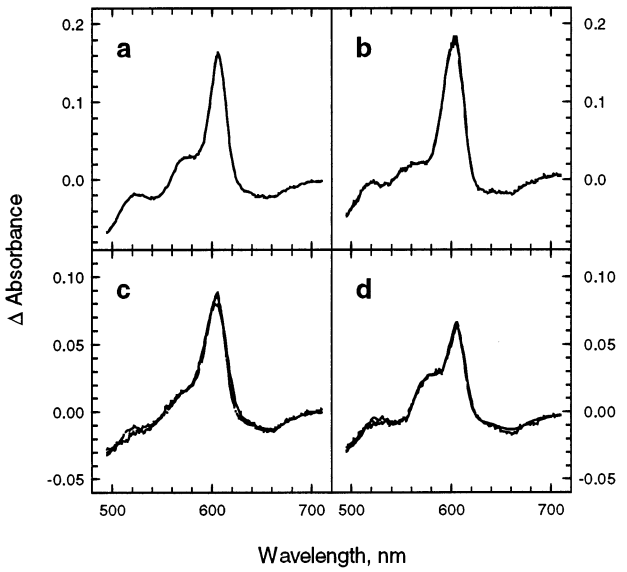

FIGURE 12: Intermediate spectra extracted from the experimental data at pH 8.5 on the basis of a unidirectional sequential scheme (**Int$_s$**) (—) and calculated equivalent intermediate spectra (**Int$_{b,r}$**) generated on the basis of the slow-**P**/fast-**F** branched scheme [f = 0.6 (—••)] and the fast-**P**/slow-**F** branched scheme [f = 0.4 (— — —)]. **Int$_s$** spectra were derived from the experimental b-spectra using the eigenvector matrix $\mathbf{V_s}$ of the kinetic matrix of the sequential scheme (eq 3). **Int$_{b,r}$** spectra were calculated on the basis of the reduced set of b-spectra (**b$_{b,r}$**) and $\mathbf{V_s}$ (eq 4). Spectra of intermediates **2**−**5** are shown in panels a−d, respectively. The spectra are referenced vs the oxidized enzyme.

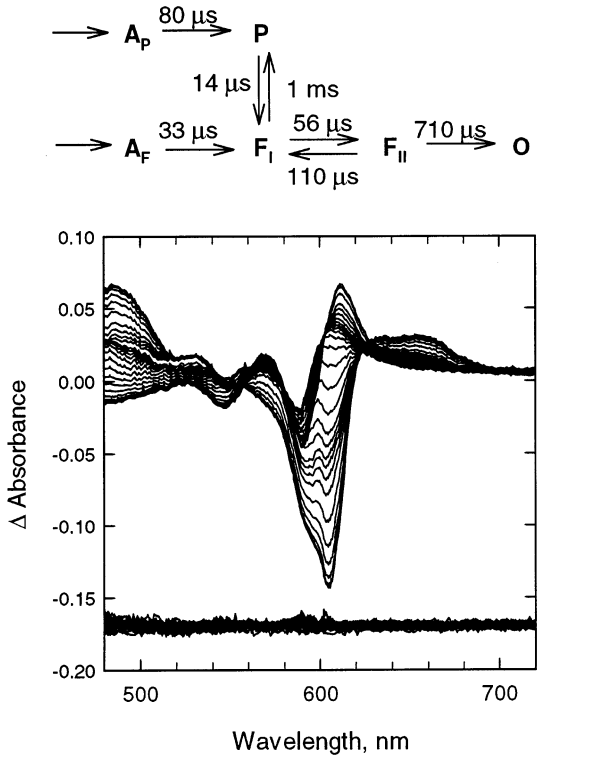

FIGURE 13: Reproduced data at pH 6.2 using the listed microscopic lifetimes (units of 10^3 s^{-1}). The residuals represent the difference between the experimental data and the reproduced data.

the 83−100 μs **b$_b$** spectrum. The remaining parts of the 50 and 83−100 μs **b$_b$** spectra were added to the 220 μs **b$_b$** spectrum to reproduce the 240 μs experimental b-spectrum. Figure 11 shows that the reduced set of b-spectra (**b$_{b,r}$**) for an f of 0.4 (— — —) are in good agreement with the experimental b-spectra (—).

Reproducing the Sequential Intermediate Spectra. The reduced number of intermediate spectra (**Int$_{b,r}$**) were calculated from the reduced set of b-spectra (**b$_{b,r}$**) according to eq 4. Figure 12 compares the spectra of intermediates **2**−**5** at an f of 0.6 for the slow-**P**/fast-**F** combination (—••) and at an f of 0.4 for the fast-**P**/slow-**F** scheme (— — —) to the intermediates derived on the basis of a unidirectional sequential model (—). It is clear that the branched scheme reproduces the sequential intermediate spectra very well. The ratios of k_{I-II} and k_{II-I} and k_{PF} and k_{FP} rates in the branched scheme are determined by the fifth intermediate. The **P**-to-**F** equilibrium is still quite forward-shifted to reproduce the minor **P** fraction observed in **Int$_s$5**. The **F$_I$**-to-**F$_{II}$** equilibrium is close to 1, less forward-shifted than at pH 6.2 and 7.5.

Reproduction of the Time-Dependent Data. A third criterion used to test the validity of the branched scheme involves a comparison between the experimental data and the reproduced data based on the branched scheme at all three pH values for both the slow-**P**/fast-**F** and fast-**P**/slow-**F** schemes. Figure 13 shows the reproduced data at pH 6.2 using the listed lifetimes. The residuals, which represent the difference between the experimental data and the reproduced data, indicate that the reproduced data match the experimental set at all delay times reasonably well. A slight deviation from the experimental data is observed near 600 nm at delay times and pH values when a significant amount of **P** is present. This is due to a slightly narrower model **P** spectrum than would be optimal for a perfect fit. A good agreement was also observed between the experimental and reproduced data at pH 7.5 and 8.5.

DISCUSSION

When kinetic data are analyzed, the events are frequently arranged in a sequence from the fastest to the slowest apparent rate on the basis of a multiexponential fit, and the apparent rates are used in place of microscopic rates to connect the intermediates. In many previous studies on cytochrome oxidase, reaction rates and spectral changes have been measured at a single wavelength or at a few selected wavelengths (*3*−*6*). This limits the spectral information, and most of the conclusions are necessarily based on the apparent rates. When the spectral amplitudes associated with the apparent rates, i.e., the b-spectra, are available, they are often incorrectly assigned to spectral changes between intermediates. This type of analysis, although useful in some cases, can only be regarded as an approximation and cannot replace a proper analysis based on a unidirectional sequential scheme, which allows one to calculate the pure spectra of the intermediate states.

The unidirectional sequential mechanism is one of the simplest schemes, and it allows a simple mathematical solution of the kinetics, making it very attractive in spectral analysis. However, it is only one of several possible alternatives. Since interpretation of kinetics on a molecular level can only be done within the framework of a kinetic mechanism, schemes that are more consistent with a variety of experimental observations are likely to lead to more reliable interpretations. We view such schemes not as final answers but rather as a framework for testing new ideas and as a guide for future work.

The branched mechanism is seemingly a complicated network, but in fact it is a simple extension of the unidirectional sequential scheme, which permits the simultaneous formation of the **A**, **P**, and **F** forms. The intermediate spectra extracted on the basis of the unidirectional sequential scheme or the equivalent experimental b-spectra are the fingerprints of the reaction, which led us to the branched model. Note that many of the microscopic rates in the branched scheme were taken directly from the experiment, and only a few rates were adjusted. The values for the variable rates were not chosen at random either. The values for the k_P and k_F pair were determined by the 30−40 μs experimental apparent lifetime and the composition of the sequential intermediate **4** (**Int$_s$4**), and the ratio of the k_{I-II} and k_{II-I} rates was set by the composition of **Int$_s$5**. The rates of the reversible step between **P** and **F** were less guided by the experimental lifetimes, but more by the experimental composition of sequential intermediate **4**.

The testing of the rather complex branched scheme by converting it into an equivalent traditional unidirectional sequential scheme represents an entirely new computational approach developed in our laboratory, which is introduced here for the first time. The testing is nontrivial due to the kinetic degeneracy and is based on linear algebra. Traditional scheme fitting techniques based on numeric integration of reaction rates describe the overall changes in a reaction without providing details of the kinetics and the spectral changes associated with each step. The algebraic kinetic analysis approach introduced here dissects the kinetic process and reveals the contribution of each individual step to the overall kinetic process and the corresponding spectral changes.

pH Dependence of the Apparent Lifetimes. The branched scheme puts the pH dependence of the apparent lifetimes and the microscopic rates into a new perspective. The microscopic rates of the early steps in the branched scheme, including the decay of compound **A**, do not depend on pH, which is consistent with the pH independence of the first three experimental apparent lifetimes (*17*, *36*, *38*, *39*). The pH dependence of the last two apparent lifetimes is interpreted differently in the branched versus the unidirectional sequential scheme. The fourth apparent lifetime (80−240 μs) is particularly interesting in this respect because it is linked to different steps in the branched scheme at different pH values. At pH 6.2, this apparent lifetime is somewhat below 100 μs and is associated with the slow decay of compound **A**. At pH 7.5, this lifetime is close to 100 μs and corresponds to the decay of both **A** and **P**. At pH 8.5, this lifetime is somewhat longer than 200 μs and is determined by the decay of **P**. Thus, in terms of the branched scheme, this apparent rate has a physically meaningful pH dependence only in the alkaline range, where it monitors the decay of **P**. In terms of the unidirectional sequential scheme, this apparent lifetime was assigned to a single molecular process and its pH dependence was explained by the titration of a group with a p*K* of 8−8.5 (*38*). This example clearly illustrates that molecular interpretations of kinetics are always intimately connected to a particular scheme, and they are valid as long as the scheme is correct.

The pH dependence of the microscopic rates in the branched scheme is easily understood. As already mentioned, the transition from **P** to **F** is favored at low pH, which is reflected in the sharp increase in the k_{PF} rate constant (∼14 times) when the pH is reduced from 8.5 to 6.2. Note that this microscopic rate constant is much more pH-dependent in the branched model than is the apparent lifetime of 80−200 μs, which is assigned to the decay of the putative $\mathbf{P_R}$ intermediate in the unidirectional sequential scheme. The two forms, **P** and **F** (Scheme 1), likely differ in the protonation state of one or more groups with a direct or indirect access to the binuclear center, which most likely has a profound effect on their visible spectra (see below).

The electron transfer from Cu_A to heme *a*, k_{I-II}, also shows significant pH dependence (*17*), suggesting a coupling between electron and proton transfer (*40*−*43*), the mechanism of which is still unknown. The equilibrium constant (k_{I-II}/k_{II-I}) for this step decreases with increasing pH, and the change corresponds to a net change in the redox potentials of heme *a* and Cu_A of 20−30 mV.

The pH dependence of the 1−2 ms apparent lifetime is far more significant than that of the k_O microscopic rate of the last step. The former primarily reflects pH-dependent rate changes in the reversible step between $\mathbf{F_I}$ and $\mathbf{F_{II}}$, rather than changes associated with the last step. When the apparent rates are assigned as microscopic rates as they frequently are in the case of the unidirectional sequential scheme, the last step inevitably becomes significantly pH dependent (*38*), which again demonstrates that the kinetic scheme largely predetermines the molecular interpretation of the reactions.

Electron Exchange between Heme a and Cu$_A$. Our estimate of the equilibrium constant for the electron transfer between heme *a* and Cu_A (k_{I-II}/k_{II-I}) falls in the range of 1.4−2.0 at neutral pH. This corresponds to a forward-shifted electron transfer from Cu_A to heme *a*, with 55−66% of heme *a* being reduced. These results are consistent with our previously reported value of ∼2.0, which was based both on spectral changes in the visible region, where heme *a* absorbs strongly (*14*), and on spectral changes in the near-infrared region, where Cu_A absorption is dominant (*15*). In a recent resonance Raman study, the oxidation state of heme *a* was monitored during the dioxygen reduction and the results were reported to be inconsistent with our previously reported equilibrium constant of ∼2.0 (*10*). The transient plateau observed in the time dependence of the scattering signal at 1518 cm^{-1}, a frequency assigned to the reduced heme *a*, corresponded to approximately 70% heme *a* being oxidized on time scales between 100 and 1000 μs. This was interpreted in terms of an equilibrium constant of 0.5, which is clearly different from our reported value of 1.4-2.0 (refs *14* and *15* and this work). We believe the reason for this apparent discrepancy arises from the misinterpretation of the resonance Raman result, where the transient plateau was identified as the establishment of the equilibrium state (*10*). The simulated time dependence of the oxidized fraction of heme *a* at pH 7.5 in Figure 15 (−) shows that at the plateau, ∼60% of heme *a* is oxidized between 100 and 1000 μs, close to that reported by Han et al. (*10*). More importantly, the simulated time dependence of heme *a* shows that equilibrium is never established. The plateau in the curve represents a transient steady state, resulting from two opposing events, the 30−40 μs and 1.4 ms processes leading to the oxidized heme *a*, and the 100 μs process leading to an equilibrated mixture of reduced and oxidized heme *a*. Note that approximately the same curve is produced whether we use the sequential model

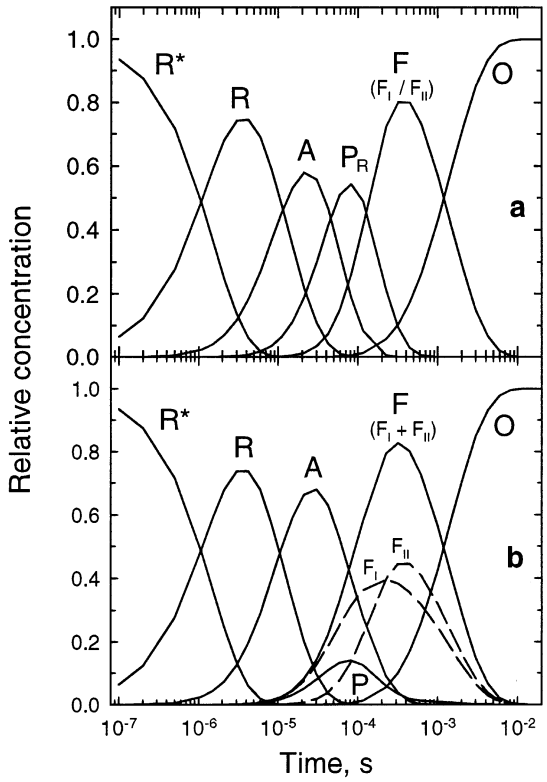

FIGURE 14: (a) Time-dependent concentration profiles of the intermediates of a unidirectional sequential scheme at pH 7.5. (b) Time-dependent concentration profiles of the intermediates in the branched scheme. The isospectral intermediates in the two branches are combined. Intermediate **4** is the putative $\mathbf{P_R}$.

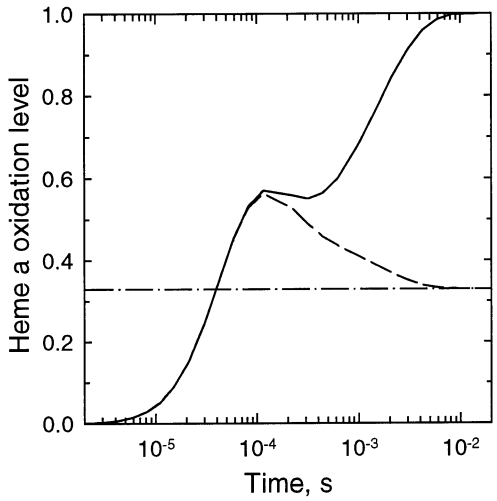

FIGURE 15: Simulated time dependence of the oxidized fraction of heme *a* at pH 7.5 (—). An equilibrium constant for the electron transfer between heme *a* and Cu_A (k_{I-II}/k_{II-I}) of 2.0 was used (*10*, *12*). Simulated time dependence of the oxidized fraction of heme *a* at pH 7.5 if the step involving the oxidation of heme *a* with a 1.4 ms lifetime is omitted (— — —). The horizontal dashed line represents the level of oxidized heme *a* if the equilibrium between $\mathbf{F_I}$ and $\mathbf{F_{II}}$ was reached.

as we did in our earlier work (*14*) or the more complex branched scheme (Figure 15) because the latter reproduces the intermediates of the former. It is quite clear that the transient plateau in this curve is well above the equilibrium line (Figure 15) which would only be reached if there were no further oxidation of heme *a* with the 1.4 ms apparent lifetime.

Multiple Ferryl States? The spectrum of intermediate **5** extracted on the basis of a unidirectional sequential scheme can be reproduced by the spectrum of the ferryl state with heme *a* and Cu_A in different proportions depending on pH (*17*). Moreover, at pH 8.5, a minor contribution of **P** was required to adequately model the spectrum. In our derivation of the branched scheme, we assumed that there was only one ferryl state of the binuclear center and that the differences between $\mathbf{F_I}$ and $\mathbf{F_{II}}$ were due to the different oxidation states of heme *a* and Cu_A in the two forms. An alternative to this hypothesis is that there is an early ferryl state, $\mathbf{F_0}$, which is practically isospectral with the subsequent $\mathbf{F_I}$ and $\mathbf{F_{II}}$ states, but with a different protein conformation. Multiple almost isospectral **F** states have been reported previously (*14*, *21*, *22*, *39*, *44*).

If the step between $\mathbf{F_0}$ and $\mathbf{F_I}$ were reversible, then this alternative scheme could not be distinguished from the branched scheme (Scheme 1) by absorption spectroscopy. The two spectrally identical and interconverting intermediates in the alternative scheme, $\mathbf{F_0}$ and $\mathbf{F_I}$, would together represent the $\mathbf{F_I}$ form in Scheme 1. However, an irreversible step from $\mathbf{F_0}$ to $\mathbf{F_I}$ would result in a new kinetic scheme that could be distinguished from Scheme 1. It is consistent with the experimental data only if the $\mathbf{F_I}$ and $\mathbf{F_{II}}$ forms are in a fast, kinetically unresolved equilibrium. In this case, the intermediate containing the unresolved mixture of the $\mathbf{F_I}$ and $\mathbf{F_{II}}$ forms would be equivalent to $\mathbf{Int_s5}$ of the unidirectional sequential model. The microscopic rate of its formation would be the sum of the two microscopic rates observed in the branched scheme (Scheme 1) for the reversible step between $\mathbf{F_I}$ and $\mathbf{F_{II}}$. Obviously, an alternative scheme involving $\mathbf{F_0}$, in addition to $\mathbf{F_I}$ and $\mathbf{F_{II}}$, does not allow any **P** form to be present at late times, and therefore reproduces the experimental data at pH 8.5 only approximately. In all other aspects, this modification of our proposed branched scheme cannot be rejected on the basis of our absorption data.

Experimental Predictions Based on the Branched Model. The branched scheme has a number of remarkable features. The most important one is, perhaps, that the kinetics can be described quantitatively by known forms of the enzyme, which can be generated on the bench. Interpreting the kinetics by a sequential scheme and identifying the intermediates with one of the known forms does not go beyond qualitative agreement, which could be observed only in the visible region (Figure 4 of ref *17*). The branched scheme is also consistent with a variety of observations, enumerated below.

*(1) Absence of **P** in Time-Resolved Resonance Raman Experiments.* The assignment of the fourth sequential intermediate generated during the dioxygen reduction to a **P** state has been controversial. In optical studies, a process is observed on a time scale of 30−40 μs, following the decay of compound **A** and long before the observation of the ferryl form at 580 nm (*4*, *6*, *13*, *14*, *45*). On the other hand, both Babcock and co-workers and Rousseau's group have not been able to detect the 804 cm^{-1} resonance Raman frequency, characteristic of the $\mathbf{P_M}$, on this time scale (*9*, *10*). Kitagawa and co-workers also failed to identify the 805 cm^{-1} band assigned to the **P** form in their time-resolved resonance studies on the reaction of the reduced cytochrome *bo* with O_2 (*46*).

These apparently conflicting results can be resolved within the context of the branched scheme. The concentration profiles of the intermediates of a unidirectional sequential scheme clearly show a substantial amount of the presumed "peroxy" form present (**Int$_s$4** in Figure 14a), and there is seemingly no reason this form could not be detected in flow-flash resonance Raman experiments on the fully reduced enzyme. However, when the time-dependent concentration profiles of the intermediates in the branched scheme are inspected (Figure 14b), it is clear that very little of the P form is actually present and its detection in resonance Raman experiments, particularly at pH 6.2, would be a formidable task. Note that the mixture of reaction products which accumulates during the reaction process and is represented by the time−concentration profiles is determined entirely by the rate constants in the reaction scheme and has no direct relation to the spectral composition of the individual intermediates. Thus, in general, the mixture of the reaction products generated at any time delay does not provide information regarding the composition of the intermediates.

(2) Resolution of the Spectral Discrepancy between ***P$_M$*** *and Intermediate* ***4*** *(****P$_R$****).* The branched scheme resolves the spectral discrepancy between **P$_M$** and intermediate **4** (**P$_R$**) (*16*) by allowing partial formation of the **F** form in one branch and retaining the **P**-to-**F** reversible transition sequence in the other branch. The scheme is thus consistent with the early observations of Wikström that the **P** form can be detected in mitochondria during reverse electron flow (*47*, *48*).

Although we were aware of the spectral differences between **P$_M$** and the putative **P$_R$** earlier (*13*, *14*, *16*), we were unable to provide a satisfactory explanation for them. In our previous publications (*13*, *14*), we explained the discrepancy in terms of simple branches; however, these models did not provide the required spectral agreement between experimental sequential intermediate **4** and the model spectra. At the time, we were unable to analyze the more complex problem of converting an extended branched model into an equivalent simple scheme, which is necessary to understand the origin of the intermediates in the simple unidirectional sequential scheme used previously by us and others.

Morgan et al. have reported that the spectra of **P$_M$** and the putative **P$_R$** are identical on the basis of optical studies at low temperatures (*49*). The reason for the difference between their data and ours was discussed in our recent paper (*16*) and will not be discussed here in detail. In short, because their double-difference spectra (the difference between the kinetic components associated with the decay of compound **A** in the fully reduced and the mixed-valence enzyme) are dominated by the large spectral change associated with the oxidation of heme *a*, important deviations that can be observed upon a direct comparison of the spectra of intermediate **4** (**P$_R$**) and **P$_M$** as in our studies (*16*) may not be observed. Moreover, the optical spectra of Morgan et al. (*49*) were recorded at −90 °C, while our data were recorded at room temperature. It is not unlikely that the relative populations of the two branches may be affected by temperature, which could provide an explanation for the difference between the two studies; i.e., at low temperatures, most of the molecules may go through the **P** branch. Further studies over a large temperature range should help resolve the differences between the two studies.

Morgan et al. also provided EPR evidence for the presence of the **P** intermediate when the fully reduced enzyme reacts with O_2 (*49*); however, the quantitation of the EPR signal was not reported. These results are not at odds with our results which show that the **P** form is indeed formed, but is only one component of three making up intermediate **4**.

(3) The Branched Scheme Is Consistent with a ***P****-to-****F*** *pH-Dependent Transition*. Fabian and Palmer have recently shown that the **P** formed at high pH decays to the **F** form when the pH is reduced, suggesting that the **P**-to-**F** transition is associated with the uptake of a proton (*23*). Our branched scheme is consistent with this finding because the microscopic rate of the **P**-to-**F** transition is the most pH-dependent one, and it increases sharply at lower pH values.

(4) The Branched Model Reproduces the 50 μs Rate of Electric Exchange between heme a and ***Cu$_A$***. The kinetic separation of the **F$_I$** and **F$_{II}$** forms is another remarkable feature of the branched scheme. When previous flow-flash data have been analyzed using a unidirectional sequential mechanism, the rate of electron transfer between heme *a* and Cu_A was not resolved (*3*−*6*, *13*, *14*). In the context of the sequential scheme, the **F$_I$** and **F$_{II}$** forms were assigned to **Int$_s$5** with an unresolved fast equilibrium between them which was observed with the same apparent lifetime, 100 μs at pH 7.5, seen for the conversion to **P** to **F** (*14*, *17*). However, the sum of the microscopic rates of the reversible step between **F$_I$** and **F$_I$** in the branched scheme (Tables 1−4) provides a lifetime of ∼50 μs, which is surprisingly close to the values observed upon photolysis of the two- and three-electron-reduced CO-bound enzyme (*11*, *12*, *35*−*37*). Note that we did not make any special effort to ensure this agreement; we only restricted the ratios of these microscopic rates in accordance with the composition of **Int$_s$5**.

The above discussion clearly shows that the branched scheme is consistent with a variety of experimental observations. We expect that time-resolved resonance Raman and time-resolved infrared experiments on the reaction of the fully reduced enzyme with O_2 over a wide pH and temperature range will provide more insight into the physical origin of the branches and will narrow the range of possibilities considered here. Site-directed mutagenesis of crucial residues in the D- and K-proton transfer pathways might also shift the equilibrium between the two branches and provide information regarding the role of specific amino acid residues in the branched pathway model. Interestingly, site-directed mutagenesis of Ser(I-299) in *Rhodobacter sphaeroides*, which is at the entry point of the K-proton transfer pathway, shows that formation of the putative **P$_R$** intermediate and the oxidation of heme *a* are not observed, and that the **A** intermediate decays directly to **F** at about the same rate as in the wild-type enzyme (*50*). This suggests that that the **P** branch may be inhibited in these mutants.

Origins of the Branched Pathways. Our studies of the reaction of the fully reduced enzyme with dioxygen at different pH values have revealed heretofore unexpected complexity which is inconsistent with the conventionally unidirectional sequential pathway (**R*** → **R** → **A** → "**P$_R$**" → **F** → **O**). Rather, the reaction appears to follow a branched mechanism, with the rate of exchange between the two branches being pH-dependent. The two branches most likely arise from different ligand or protein conformers, with different accessibility of proton donors to the binuclear

center. Multiple ligand conformers have been observed in the IR, FTIR, and resonance Raman spectra of heme-copper oxidases from various species, when CO is bound to heme a_3 and following its photodissociation and binding to Cu_B (*51*−*60*). These conformers have also been observed in the CO-FTIR spectra of mitochondrial membranes (*51*, *52*, *61*) and intact plasma membranes (*62*). The CO-FTIR experiments have indicated that the conformers interconvert rapidly (*53*, *63*) and therefore cannot be isolated as structurally different conformers. Thus, while the nature of these conformers is unknown, the conformers appear to be a characteristic of the enzyme, and not an artifact due to removal of the enzyme from the membrane or isolation procedure. Multiple pH- and temperature-dependent rapidly interconverting CO and O_2 conformers have also been reported for hemoglobin and myoglobin (*64*, *65*).

The two pathways may result from different conformations of protonated amino acid(s) in response to ligand state changes. FTIR studies of fully reduced cytochrome bo_3 from *Escherichia coli* at cryogenic temperatures have shown that binding of CO to Cu_B following CO photolysis from heme o_3 is associated with changes in the environment around glutamic acid 242, E242 (bovine heart oxidase numbering), in the D-pathway (*66*), a critical conserved residue in subunit I. Recent FTIR studies (*59*) and time-resolved step-scan FTIR studies on the bovine heart enzyme (*67*, *68*) have shown a similar or the same spectroscopic perturbation in bovine heart cytochrome oxidase at −20 °C, 9 °C, and room temperature.

FTIR data indicate that E242 is fully protonated in the reduced and CO-bound forms of the enzyme (*66*, *69*), and the changes in the environment of E242 observed in FTIR upon photodissociation of CO from heme a_3 (heme o_3) and its subsequent binding to Cu_B have been interpreted in terms of hydrogen-bonded connectivity between E242 and Cu_B (*66*). The proton conduction or proton shuttling from E242 to the binuclear center has been suggested to involve a conformational isomerization of the side chain of this amino acid (*2*, *70*−*73*), which has been proposed to be important in the proton translocation mechanism of the enzyme (*66*, *70*). The two-branch model may therefore represent two similar energy conformations of the Cu_B−CO-bound or the heme a_3−O_2-bound enzyme which differ with respect to the orientation of the side chain of E242 (*71*, *72*). Interestingly, FTIR H−D exchange experiments by Rich and co-workers (*59*) have provided evidence for the perturbation of at least two carboxylic acid residues or the same residue in different environments following photodissociation of CO from heme a_3. These findings have been supported by time-resolved step-scan FTIR experiments (*68*), which furthermore showed that the perturbation in the carboxyl region upon light-induced dissociation of CO from heme a_3 and ligation to Cu_B persisted well beyond the time scale for the dissociation of CO from Cu_B. The two conformations could have different accessibilities to protons or have different abilities to compensate for protonation and/or deprotonation or electron transfer events at the binuclear center. Another possible amino acid that might be affected by conformational changes at the binuclear center is the cross-linked tyrosine, which has been proposed to act as a proton and electron donor upon breaking of the dioxygen bond (*14*, *33*, *74*, *75*).

At What Step Does the Branching Occur? As noted earlier, it is unclear whether the branching occurs upon photolysis (Scheme 1a) or whether the two branches have a common origin and branch into the two pathways at either **R*** (Scheme 1b) or **R** (Scheme 1c). If the photolysis of CO and subsequent binding of CO to Cu_B lead to a carboxyl acid residue in two different conformational states, two isospectral **R*** states would be observed (Scheme 1a). It is also possible that the two conformations arise during O_2 binding to Cu_B or heme a_3, in which case the two pathways would branch at **R** (Scheme 1c). Regardless, the two pathways (branches) have distinct heme a_3−O_2 intermediates, $\mathbf{A_P}$ and $\mathbf{A_F}$, respectively, which are isospectral but kinetically not equivalent. A conformational change in an amino acid located some distance from the binuclear center could significantly affect the kinetics of electron and/or proton transfer, without significantly affecting the spectral properties.

For both the slow-**P**/fast-**F** and fast-**P**/slow-**F** alternatives, the majority of the molecules go through the slow branch. The fraction of molecules going through the **P** branch for the slow-**P**/fast-**F** scheme is 0.7−0.85, 0.5−0.75, and 0.6−0.7 at pH 6.2, 7.5, and 8.5, respectively, which indicates that a slightly higher fraction of molecules go through the slower branch at the lower pH. Almost identical values were obtained for the number of molecules going through the **F** branch in the fast-**P**/slow-**F** branched scheme. A stronger pH dependence is observed for the conversion of **P** to **F**, where k_{PF} is more than 10 times larger at pH 6.2 than at pH 8.5 to reflect the larger percentage of **F** at the lower pH. The proton required for the formation of **F** may come from E242 in the appropriate conformation, while in a different conformation, this process cannot occur. Mutations of residue E242 have been shown to affect several steps in the catalytic cycle, including the conversion of the putative $\mathbf{P_R}$ to **F** and **F** to **O** (*40*, *43*, *73*, *76*).

Branched pathways have been proposed previously on the basis of time-resolved resonance Raman studies of the reaction of the fully reduced cytochrome oxidase with dioxygen (*1*, *10*, *77*), but detailed kinetic and spectral analysis has been lacking. These schemes usually involve a branch for the formation of the peroxy intermediate in the mixed-valence enzyme ($\mathbf{P_M}$) and another one for the formation of the putative $\mathbf{P_R}$ intermediate in the reduced enzyme. As discussed above, neither the East Lansing group nor the Bell group has observed the 804 cm^{-1} **P** species in flow-flash time-resolved resonance Raman experiments on the fully reduced enzyme (*9*, *10*). Both groups have suggested that the **P** intermediate is not populated to a great extent in the flow-flash experiments on the fully reduced enzyme (*1*, *10*), which is consistent with the concentration profiles of the intermediates in the branched scheme (Figure 14b), but inconsistent with the profiles for the unidirectional sequential scheme (Figure 14a). Han et al. (*10*) have also recently reported that the oxoferryl mode at 786 cm^{-1} (**F**) is observed on the same or a similar time scale as the oxidation of heme *a*. These results are consistent with our observations that the **F** intermediate is indeed a component of intermediate **4** present in the unidirectional sequential mechanism. Thus, our branched pathway model provides experimental support for many of the previous time-resolved resonance Raman observations.

Reaction of the Oxidized Enzyme with H_2O_2 Also Follows a Branched Pathway. The reaction of fully reduced cytochrome oxidase with O_2 shows interesting parallels with the

reaction of the oxidized enzyme with H_2O_2. The latter reaction has been reported to produce predominantly **P** at high pH and **F** at low pH (*18*−*24*). The reactions of H_2O_2 with oxidized cytochrome bo_3 from *E. coli* (*21*, *78*) and with bovine heart cytochrome oxidase (*22*) both provide strong evidence for a pH-dependent branching mechanism at either the **P** state (*21*, *78*) or the oxidized state (*22*) and the formation of two oxyferryl forms. Pecoraro et al. (*24*) recently reported that at high pH (8.5), the reaction of oxidized cytochrome oxidase from *Rhodobacter sphaeroides* with H_2O_2 produces an intermediate that is a mixture of the 607 nm **P** form and the 580 nm **F** form, while at acidic pH (6.5), only an **F** intermediate (∼575 nm) was observed. A pH-dependent branched pathway was proposed that involved the formation of **P** and the subsequent formation of **F** in the alkaline branch and the formation of a second **F** form in the acidic branch (*24*). Mutation of the critical lysine 362 indicated that the formation of the **F** form at acidic pH required proton uptake through the K channel (*24*).

Both the branched scheme reported here and the branched reaction scheme reported for the reaction of cytochrome oxidase with H_2O_2 (*21*, *22*, *24*, *78*) involve the formation of **P** in one branch and **F** in the other. Thus, branching mechanisms could be a more general property of the enzyme than previously thought. The two reactions of course differ with respect to the branching point. In the reaction of the enzyme with H_2O_2, the branching point is the oxidized (*22*, *24*) or **P** state (*22*), while in the reaction of the reduced enzyme with dioxygen, the branching point precedes the formation of the two isospectral $\mathbf{A_P}$ and $\mathbf{A_F}$ intermediates. This probably indicates different physical origins of the two branches in the two different reactions. Also, two ferryl (**F**) species are proposed for the reaction of oxidase with H_2O_2, while our branched scheme includes only one ferryl. Although our data modeling does not require or resolve spectrally similar but nonidentical oxyferryl forms, we cannot exclude this possibility. If two spectrally similar ferryl forms were indeed generated during the reaction of the reduced enzyme with O_2, our scheme would become more complex and more similar to that proposed for the reaction of the oxidized enzyme with H_2O_2 (*22*, *24*). Finally, the **P** form generated during the reaction of H_2O_2 with cytochrome oxidase is slowly converted to the **F** form upon proton uptake (*22*−*24*), while the conversion of **P** to **F** is fast during the reduction of dioxygen to water. The differences between the two results most likely arise from the extra electron in the reduced enzyme, which possibly converts the neutral tyrosine radical in $\mathbf{P_M}$ to tyrosinate.

P_M Is Formed through a Sequential Unidirectional Mechanism. In the flow-flash reaction of dioxygen with the mixed-valence enzyme, the $\mathbf{P_M}$ intermediate is observed as the final product (*16*); i.e., the formation of $\mathbf{P_M}$ follows a unidirectional sequential mechanism and not a branched pathway (*16*). One explanation for this is that the protein conformers present in the fully reduced enzyme are linked to the redox state of heme *a*. This is supported by FTIR studies which have shown spectral changes in the carboxyl residue region (attributed to E242) with a change in the redox state of heme *a* (*79*−*81*). Alternatively, both $\mathbf{A_P}$ and $\mathbf{A_F}$ could be present in the mixed-valence enzyme, with $\mathbf{A_F}$ not being converted to **F** because of the lack of the availability of a proton. This scenario would require an equilibrium between $\mathbf{A_P}$ and $\mathbf{A_F}$ on a time scale similar to that of the decay of $\mathbf{A_P}$ to **P**. In the fully reduced enzyme, the time scale of the decay of $\mathbf{A_P}$ to **P** is either 30 or 100 μs, and therefore may preclude the detection of the equilibrium between $\mathbf{A_P}$ and $\mathbf{A_F}$.

CONCLUSIONS

Our data suggest that the spectrum of the putative intermediate $\mathbf{P_R}$ state is a pH-dependent superposition of three spectra corresponding to **A**, **P**, and **F** (*17*). At alkaline pH, all three forms are present, while at more acidic pH, the formation of **F** is favored over **P**. Our mathematical modeling in terms of a branched mechanism accounts for these findings.

The branched scheme, as any other kinetic scheme, is a simplified description of the many temporal changes occurring in a multistep chemical reaction. A valid kinetic scheme is consistent with the experimental observations but does not exclude other interpretations; in other words, a kinetic scheme cannot be proven. To address the question of uniqueness, we introduced from the start both the slow-**P**/fast-**F** and fast-**P**/slow-**F** alternative versions, showing the range of microscopic rates consistent with the experimental data. The novel algebraic procedure presented here allows us to see the contribution of each step to the global kinetic picture as well as to each of the components of the global exponential fit. It also allows us to evaluate the effects of close reaction rates and isospectral forms on the kinetic data of cytochrome oxidase. Further experimental evidence may favor one version or the other and narrow the range of *f* values and microscopic rates. However, we believe that the mechanism of branched pathways remains the basis for future interpretations. In our best judgment, this mechanism is the most consistent with the current information on the reduction of dioxygen to water by the fully reduced enzyme. Our mathematical approach can now be extended to other biological systems where the complexity is greater than what can be described by a simple unidirectional sequential mechanism.

REFERENCES

1. Ferguson-Miller, S., and Babcock, G. T. (1996) *Chem. Rev. 96*, 2889−2907.
2. Zaslavsky, D., and Gennis, R. B. (2000) *Biochim. Biophys. Acta 1458*, 164−179.
3. Hill, B. C., and Greenwood, C. (1984) *Biochem. J. 218*, 913−921.
4. Oliveberg, M., Brzezinski, P., and Malmström, B. G. (1989) *Biochim. Biophys. Acta 977*, 322−328.
5. Hill, B. C. (1994) *J. Biol. Chem. 269*, 2419−2425.
6. Verkhovsky, M. I., Morgan, J. E., and Wikström, M. (1994) *Biochemistry 33*, 3079−3086.
7. Han, S., Ching, Y.-C., and Rousseau, D. L. (1990) *Nature 348*, 89−90.
8. Ogura, T., Takahashi, S., Hirota, S., Shinzawa-Itoh, K., Yoshikawa, S., Appleman, E. H., and Kitagawa, T. (1993) *J. Am. Chem. Soc. 115*, 8527−8536.
9. Varotsis, C., Zhang, Y., Appelman, E. H., and Babcock, G. T. (1993) *Proc. Natl. Acad. Sci. U.S.A. 90*, 237−241.
10. Han, S., Takahashi, S., and Rousseau, D. L. (2000) *J. Biol. Chem. 275*, 1910−1919.
11. Georgiadis, K. E., Jhon, N.-I., and Einarsdóttir, Ó. (1994) *Biochemistry 33*, 9245−9256.
12. Einarsdóttir, Ó., Georgiadis, K. E., and Sucheta, A. (1995) *Biochemistry 34*, 496−508.

13. Sucheta, A., Georgiadis, K. E., and Einarsdóttir, Ó. (1997) *Biochemistry 36*, 554−565.
14. Sucheta, A., Szundi, I., and Einarsdóttir, Ó. (1998) *Biochemistry 37*, 17905−17914.
15. Szundi, I., Liao, G.-L., and Einarsdóttir, Ó. (2001) *Biochemistry 40*, 2332−2339.
16. Einarsdóttir, Ó., Szundi, I., Van Eps, N., and Sucheta, A. S. (2002) *J. Inorg. Biochem. 91*, 87−93.
17. Van Eps, N., Szundi, I., and Einarsdóttir, Ó. (2003) *Biochemistry 42*, 5065−5073.
18. Wrigglesworth, J. M. (1984) *Biochem. J. 217*, 715−719.
19. Weng, L., and Baker, G. M. (1991) *Biochemistry 30*, 5727−5733.
20. Fabian, M., and Palmer, G. (1995) *Biochemistry 34*, 13802−13810.
21. Brittain, T., Little, R. H., Greenwood, C., and Watmough, N. J. (1996) *FEBS Lett. 399*, 21−25.
22. Jünemann, S., Heathcote, P., and Rich, P. R. (2000) *Biochim. Biophys. Acta 1456*, 56−66.
23. Fabian, M., and Palmer, F. (2001) *Biochemistry 40*, 1867−1874.
24. Pecoraro, C., Gennis, R. B., Vygodina, T. V., and Konstantinov, A. A. (2001) *Biochemistry 40*, 9695−9708.
25. Hug, S. J., Lewis, J. W., Einterz, C. M., Thorgeirsson, T. E., and Kliger, D. S. (1990) *Biochemistry 29*, 1475−1485.
26. Henry, E. R., and Hofrichter, J. (1992) *Methods Enzymol. 210*, 129−193.
27. Thorgeirsson, T. E., Lewis, J. W., Wallace-Williams, S. E., and Kliger, D. S. (1993) *Biochemistry 32*, 13861−13872.
28. Szundi, I., Lewis, J. W., and Kliger, D. S. (1997) *Biophys. J. 73*, 688−702.
29. Slutter, C. E., Sanders, D., Wittung, P., Malmström, B. G., Aasa, R., Richards, J. H., Gray, H. B., and Fee, J. A. (1996) *Biochemistry 35*, 3387−3395.
30. Proshlyakov, D. A., Ogura, T., Shinzawa-Itoh, K., Yoshikawa, S., Appelman, E. H., and Kitagawa, T. (1994) *J. Biol. Chem. 269*, 29385−29388.
31. Proshlyakov, D. A., Ogura, T., Shinzawa-Itoh, K., Yoshikawa, S., and Kitagawa, T. (1996) *Biochemistry 35*, 76−82.
32. Proshlyakov, D. A., Ogura, T., Shinzawa-Itoh, K., Yoshikawa, S., and Kitagawa, T. (1996) *Biochemistry 35*, 8580−8586.
33. Proshlyakov, D. A., Pressler, M. A., and Babcock, G. T. (1998) *Proc. Natl. Acad. Sci. U.S.A. 95*, 8020−8025.
34. Fabian, M., Wong, W. W., Gennis, R. B., and Palmer, G. (1999) *Proc. Natl. Acad. Sci. U.S.A. 96*, 13114−13117.
35. Morgan, J. E., Li, P. M., Jang, D.-J., El-Sayed, M. A., and Chan, S. I. (1989) *Biochemistry 28*, 6975−6983.
36. Oliveberg, M., and Malmström, B. G. (1991) *Biochemistry 30*, 7053−7057.
37. Verkhovsky, M. I., Morgan, J. E., and Wikström, M. (1992) *Biochemistry 31*, 11860−11863.
38. Hallén, S., and Nilsson, T. (1992) *Biochemistry 31*, 11853−11859.
39. Paula, S., Sucheta, A., Szundi, I., and Einarsdóttir, Ó. (1999) *Biochemistry 38*, 3025−3033.
40. Ädelroth, P., Ek, M. S., Mitchell, D. M., Gennis, R. B., and Brzezinski, P. (1997) *Biochemistry 36*, 13824−13829.
41. Hallén, S., Brzezinski, P., and Malmström, B. G. (1994) *Biochemistry 33*, 1467−1472.
42. Karpefors, M., Ädelroth, P., Zhen, Y., Ferguson-Miller, S., and Brzezinski, P. (1998) *Proc. Natl. Acad. Sci. U.S.A. 95*, 13606−13611.
43. Ädelroth, P., Karpefors, M., Gilderson, G., Tomson, F. L., Gennis, R. B., and Brzezinski, P. (2000) *Biochim. Biophys. Acta 1459*, 533−539.
44. Watmough, N. J., Cheesman, M. R., Greenwood, C., and Thomson, A. J. (1994) *Biochem. J. 300*, 469−475.
45. Morgan, J. E., Verkhovsky, M. I., and Wikström, M. (1996) *Biochemistry 35*, 12235−12240.
46. Hirota, S., Mogi, T., Ogura, T., Hirano, T., Anraku, Y., and Kitagawa, T. (1994) *FEBS Lett. 352*, 67−70.
47. Wikström, M. (1981) *Proc. Natl. Acad. Sci. U.S.A. 78*, 4051−4054.
48. Wikström, M., and Morgan, J. E. (1992) *J. Biol. Chem. 267*, 10266−10273.
49. Morgan, J. E., Verkhovsky, M. I., Palmer, G., and Wikström, M. (2001) *Biochemistry 40*, 6882−6892.
50. Brändén, M., Sigurdsson, J., Namslauer, A., Gennis, R. B., Ädelroth, P., and Brzezinski, P. (2001) *Proc. Natl. Acad. Sci. U.S.A. 98*, 5013−5018.
51. Alben, J. O., Moh, P. P., Fiamingo, F. G., and Altschuld, R. A. (1981) *Proc. Natl. Acad. Sci. U.S.A. 78*, 234−237.
52. Fiamingo, F. G., Altschuld, R. A., Moh, P. P., and Alben, J. O. (1982) *J. Biol. Chem. 257*, 1639−1650.
53. Yoshikawa, S., and Caughey, W. S. (1982) *J. Biol. Chem. 257*, 412−420.
54. Einarsdóttir, Ó., Killough, P. M., Fee, J. A., and Woodruff, W. H. (1989) *J. Biol. Chem. 264*, 2405−2408.
55. Einarsdóttir, Ó., Dyer, R. B., Lemon, D. D., Killough, P. M., Hubig, S. M., Atherton, S. J., López-Garriga, J. J., Palmer, G., and Woodruff, W. H. (1993) *Biochemistry 32*, 12013−12024.
56. Wang, J., Takahashi, S., Hosler, J. P., Mitchell, D. M., Ferguson-Miller, S., Gennis, R. B., and Rousseau, D. L. (1995) *Biochemistry 34*, 9819−9825.
57. Mitchell, D. M., Müller, J. D., Gennis, R. B., and Nienhaus, G. U. (1996) *Biochemistry 35*, 16782−16788.
58. Rost, B., Behr, J., Hellwig, P., Richter, O. M., Ludwig, B., Michel, H., and Mäntele, W. (1999) *Biochemistry 38*, 7565−7571.
59. Rich, P. R., and Breton, J. (2001) *Biochemistry 40*, 6441−6449.
60. Das, K. D., Tomson, F. L., Gennis, R. B., Gordon, M., and Rousseau, D. L. (2001) *Biophys. J. 80*, 2039−2045.
61. Young, L. J., Einarsdóttir, Ó., Vossbrink, C. R., and Caughey, W. S. (1984) *Biochem. Biophys. Res. Commun. 123*, 247−253.
62. Fee, J. A., Kuila, D., Mather, M. W., and Yoshida, T. (1986) *Biochim. Biophys. Acta 853*, 153−185.
63. Einarsdóttir, Ó., Choc, M. G., Weldon, S., and Caughey, W. S. (1988) *J. Biol. Chem. 263*, 13641−13654.
64. Shimada, H., and Caughey, W. S. (1982) *J. Biol. Chem. 257*, 11893−11900.
65. Potter, W. T., Tucker, M. P., Houtchens, R. A., and Caughey, W. S. (1987) *Biochemistry 26*, 4699−4707.
66. Puustinen, A., Bailey, J. A., Dyer, R. B., Mecklenburg, S. L., Wikström, M., and Woodruff, W. H. (1997) *Biochemistry 36*, 13195−13200.
67. Heitbrink, D., Sigurdson, H., Bolwien, C., Brzezinski, P., and Heberle, J. (2002) *Biophys. J. 82*, 1−10.
68. Bailey, J. A., Tomson, F. L., Mecklenburg, S. L., MacDonald, G. M., Katsonouri, A., Puustinen, A., Gennis, R. B., Woodruff, W. H., and Dyer, R. B. (2002) *Biochemistry 41*, 2675−2683.
69. Rich, P. R., Breton, J., Jünemann, S., and Heathcote, P. (2000) *Biochim. Biophys. Acta 1459*, 475−480.
70. Riistama, S., Hummer, G., Puustinen, A., Dyer, R. B., Woodruff, W. H., and Wikström, M. (1997) *FEBS Lett. 414*, 275−280.
71. Pomès, R., Hummer, G., and Wikström, W. (1998) *Biochim. Biophys. Acta 1365*, 255−260.
72. Hofacker, I., and Schulten, K. (1998) *Proteins: Struct., Funct., Genet. 30*, 100−107.
73. Jünemann, S., Meunier, B., Fisher, N., and Rich, P. R. (1999) *Biochemistry 38*, 5248−5255.
74. Gennis, R. B. (1998) *Biochim. Biophys. Acta 1365*, 241−248.
75. Proshlyakov, D. A., Pressler, M. A., DeMaso, C., Leykam, J. F., DeWitt, D. L., and Babcock, G. T. (2000) *Science 290*, 1588−1591.
76. Watmough, N. J., Katsonouri, A., Little, R. H., Osborne, J. P., Furlong-Nickels, E., Gennis, R. B., Brittain, T., and Greenwood, C. (1997) *Biochemistry 36*, 13736−13742.
77. Han, S., Ching, Y.-C., and Rousseau, D. L. (1990) *Proc. Natl. Acad. Sci. U.S.A. 87*, 8408−8412.
78. Uchida, T., Mogi, T., and Kitagawa, T. (2000) *Biochemistry 39*, 6669−6678.
79. Hellwig, P., Behr, J., Ostermeier, C., Richter, O. M., Pfitzner, U., Odenwald, A., Ludwig, B., Michel, H., and Mäntele, W. (1998) *Biochemistry 37*, 7390−7399.
80. Lübben, M., Prutsch, A., Mamat, B., and Gerwert, K. (1999) *Biochemistry 38*, 2048−2056.
81. Hellvig, P., Rost, B., and Mäntele, W. (2001) *Spectrochim. Acta, Part A 57*, 1123−1131.

BI020483E